

CENTENNIAL FEATURE ARTICLE

Resonance Raman and Resonance Hyper-Raman Intensities: Structure and Dynamics of Molecular Excited States in Solution[†]Anne Myers Kelley[‡]

School of Natural Sciences, University of California, Merced, P.O. Box 2039, Merced, California 95344

Received: June 23, 2008; Revised Manuscript Received: August 18, 2008

Resonance Raman scattering is discussed as a vibronic spectroscopy that can provide detailed information about the structure and dynamics of excited electronic states of molecules. The emphasis is on molecules in liquid solution. The theory of resonance Raman intensities and experimental and interpretive methods are discussed both in a historical context and in their present and future implementations. The related but much less developed technique of two-photon-resonant hyper-Raman scattering is also discussed in a similar context.

Introduction

Raman spectroscopy is a form of inelastic light scattering in which a sample is irradiated with nearly monochromatic light of frequency ω_L and the frequency spectrum of the spontaneously scattered light (ω_S) is measured. Although the elastic scattering ($\omega_S = \omega_L$) is often dominant, most materials also exhibit some inelastic scattering ($\omega_S \neq \omega_L$) in which the energy difference between incident and scattered photons is provided or taken up by the material. When the increase or decrease in photon energy corresponds to excitation or deexcitation of an internal degree of freedom of the material system (rotational, vibrational, or electronic), the process is known as Raman scattering. This article addresses only vibrational Raman scattering, where the initial and final states of the material system belong to the same (usually ground) electronic state but differ in the quantum states of one or more molecular vibrations. In this case, the spectrum of scattered light intensity versus Raman shift, $|\omega_L - \omega_S|$, shows peaks at vibrational frequencies.

In general, energy may be transferred either from the electromagnetic field to the molecule or vice versa. In the first case, $\omega_S < \omega_L$ and the process is known as Stokes Raman scattering; in the second case, $\omega_S > \omega_L$ and the process is known as anti-Stokes Raman scattering (Figure 1). For most vibrations of most molecules at or below room temperature the vibrational partition function places most of the thermal equilibrium population in the ground state, so anti-Stokes scattering is weak. Therefore most Raman experiments detect scattering only on the Stokes side (scattered light lower in frequency or longer in wavelength than the exciting light). Raman scattering may generally involve a change of a single vibrational quantum in a single normal mode (fundamental), more than one vibrational

quantum in a single mode (overtone), or one or more quanta in more than one mode (combination band).

Although Raman scattering may be performed on nearly any state of matter, this article focuses on applications to molecules in liquid solution. In a typical Raman experiment the exciting light is incident on the sample in the form of a collimated or focused laser beam and the scattering is collected over a cone of angles centered around a different direction from that of the exciting beam, often 90° (right angle geometry) or close to 180° (backscattering geometry). In an isotropic liquid the contributions from each individual scatterer add incoherently, i.e., at the level of the scattered intensity rather than the scattered electric field. The angular distribution of the scattering from an isotropic sample depends only on the polarization of the scattering, which is a function of the molecular structure, the symmetry species to which the excited vibration belongs, and electronic resonance conditions.

In a Raman process an incident electromagnetic field at frequency ω_L , polarized with its electric field along the ρ direction in the molecule-fixed frame, induces a polarization in the molecule at frequency ω_S with electric field polarized along the λ direction in the molecule-fixed frame. Raman scattering is therefore described by a polarizability tensor, $\alpha(\omega_L, \omega_S)$, which in general has nine elements. In the traditional sum-over-states picture (vide infra), the elements of the Raman polarizability that contribute to a transition between molecular states $|i\rangle$ and $|f\rangle$ are given by¹

$$\alpha_{\rho\lambda, i \rightarrow f}(\omega_L, \omega_S) = \sum_v \left\{ \frac{\langle f | r_\rho | v \rangle \langle v | r_\lambda | i \rangle}{\omega_L - \omega_{vi} + i\tilde{\Gamma}_{iv}} + \frac{\langle f | r_\lambda | v \rangle \langle v | r_\rho | i \rangle}{\omega_{vi} + \omega_S + i\tilde{\Gamma}_{iv}} \right\} \quad (1)$$

where r_ρ and r_λ are vector components of the transition length operator, ω_L and ω_S are the incident and scattered wave numbers, ω_{vi} is the $|i\rangle$ to $|v\rangle$ transition frequency in wave numbers, $\tilde{\Gamma}_{iv}$ is the homogeneous line width of the $|i\rangle$ to $|v\rangle$ molecular transition in wave numbers, and the sum over v runs over all excited states of the molecule. The Raman polarizability has units of volume (cm³). The first term in eq 1 corresponds

[†] This year marks the Centennial of the American Chemical Society's Division of Physical Chemistry. To celebrate and to highlight the field of physical chemistry from both historical and future perspectives, *The Journal of Physical Chemistry* is publishing a special series of Centennial Feature Articles. These articles are invited contributions from current and former officers and members of the Physical Chemistry Division Executive Committee and from *J. Phys. Chem.* Senior Editors.

[‡] E-mail: amkelley@ucmerced.edu.

Anne Myers Kelley was born Anne B. Myers in Riverside, California, in 1958, entered the University of California, Riverside, as a biology major and left with a B.S. in chemistry in 1980. She earned a Ph.D. in biophysical chemistry with Rich Mathies at Berkeley in 1984, spent two years as an NIH postdoctoral fellow with Robin Hochstrasser at Penn, and joined the faculty in the chemistry department at the University of Rochester, moving through the ranks to Professor. In 1999 she married David F. Kelley and moved to Kansas State University, and in 2003 she became one of the first eight founding faculty of the University of California, Merced, where she now leads the undergraduate and graduate programs in chemistry. She is the author of more than 130 published papers, mainly in experimental and theoretical aspects of linear and nonlinear resonance Raman spectroscopy. She qualified for the U.S. Olympic Trials in the marathon in 1992 and still enjoys distance running at a less competitive level.

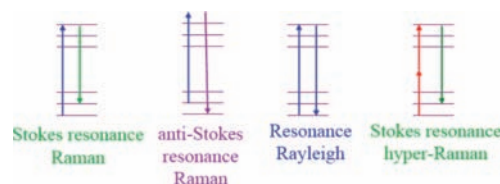


Figure 1. Energy level diagrams for Stokes and anti-Stokes resonance Raman, resonance Rayleigh, and Stokes resonance hyper-Raman processes.

to the path through state space in which the incident photon is destroyed before the scattered photon is created, the second term to the path in which the opposite time ordering holds.

The relationship between the components of α and what is actually measured in the laboratory depends on the polarization and propagation directions of the incident and scattered electromagnetic fields, and is often expressed in terms of the three Raman tensor invariants for randomly oriented molecules:¹

$$\Sigma^0 = \frac{1}{3}|\alpha_{xx} + \alpha_{yy} + \alpha_{zz}|^2 \quad (2a)$$

$$\Sigma^1 = \frac{1}{2}\{|\alpha_{xy} - \alpha_{yx}|^2 + |\alpha_{xz} - \alpha_{zx}|^2 + |\alpha_{yz} - \alpha_{zy}|^2\} \quad (2b)$$

$$\Sigma^2 = \frac{1}{2}\{|\alpha_{xy} + \alpha_{yx}|^2 + |\alpha_{xz} + \alpha_{zx}|^2 + |\alpha_{yz} + \alpha_{zy}|^2\} + \frac{1}{3}\{|\alpha_{xx} - \alpha_{yy}|^2 + |\alpha_{xx} - \alpha_{zz}|^2 + |\alpha_{yy} - \alpha_{zz}|^2\} \quad (2c)$$

For the common case of linearly polarized excitation with detection of all scattered polarizations in a direction perpendicular to the incident polarization, the Raman differential cross section (units of $\text{cm}^2 \text{steradian}^{-1}$) is given by¹

$$\left(\frac{d\sigma_{i-f}}{d\Omega}\right) = 4\pi^2\alpha^2\omega_L\omega_S^3 \frac{1}{30}(10\Sigma^0 + 5\Sigma^1 + 7\Sigma^2) \quad (3)$$

where α is the dimensionless fine structure constant. The incident laser intensity I_L (units of photons $\text{s}^{-1} \text{cm}^{-2}$) and the Raman scattered power P_{i-f} (units of photons s^{-1}) are related through the differential Raman cross section as follows:

$$P_{i-f} = I_L N \int d\Omega \left(\frac{d\sigma_{i-f}}{d\Omega}\right) \quad (4)$$

where N is the number of molecules in the illuminated volume and the integral is over the solid angle of collection (Figure 2). Note that because this equation refers to the total scattered power arising from a particular $|i\rangle$ to $|f\rangle$ Raman transition, integration over all scattered frequencies that contribute to that Raman line is assumed. In addition, if there is significant thermal population in initial states other than the vibrational ground state, all of the $|i\rangle$ to $|i+1\rangle$ transitions in a given mode will appear at approximately the same frequency and their contributions to the total scattered power must be calculated separately, weighted by the Boltzmann population of each initial state, and summed. The Raman scattered power is linear in the concentration of scatterers once corrections are made for any absorption of the incident or scattered light by the sample. It is also linear in the incident laser intensity in the absence of confounding processes such as heating of the sample by the laser or depletion of the ground-state population through electronic excitation.

In "normal" Raman scattering, the incident laser frequency is far from any molecular electronic resonance and is not absorbed by the sample. The Raman polarizabilities can be

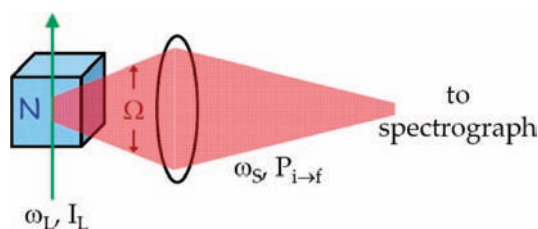


Figure 2. Schematic of Raman excitation and detection setup for the common 90° scattering geometry.

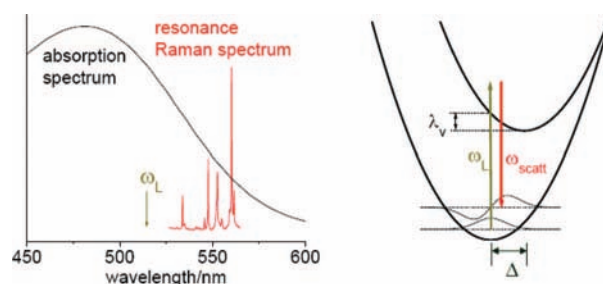


Figure 3. Left: broad, featureless optical absorption spectrum characteristic of many large molecules in fluid solution (black), and the resonance Raman spectrum obtained from this molecule by exciting with narrow-band laser at frequency ω_L (red). Though the absorption spectrum shows no vibronic structure, the resonance Raman spectrum has dozens of resolved peaks whose intensities report on the potential energy surface for the resonant excited state projected onto a specific ground-state normal coordinate. Right: one-dimensional cut through the $(3N - 6)$ -dimensional ground- and excited-state potential surfaces for an N -atom molecule. Δ is the displacement between ground- and excited-state surfaces along the selected vibrational normal coordinate, usually reported in dimensionless normal coordinates. The Huang–Rhys factor S , the ratio of the $0 \rightarrow 1$ to $0 \rightarrow 0$ Franck–Condon factors, is given by $S = \Delta^2/2$.

obtained by expanding the static molecular polarizability as a Taylor series in the vibrational coordinates. This leads to the familiar result that the Raman intensity in a given vibrational mode depends on the derivative of the molecular polarizability along that mode.^{2,3} Away from electronic resonance, polarizabilities and polarizability derivatives are usually considered properties of the electronic ground state. When the incident frequency approaches resonance with an allowed electronic transition, however, that electronic state begins to dominate the sum in eq 1 and the assumptions that go into the usual ground-state polarizability derivative picture break down. As described below, resonance Raman scattering is best considered as a vibronic spectroscopy (Figure 3). The peaks in the plot of intensity versus Raman shift still occur at ground-state vibrational frequencies, but the intensities of the Raman lines now carry specific information about the structure and dynamics of the resonant electronic state.^{4–7} The resonance Raman excitation profile, which is a plot of the cross-section for a particular Raman transition as a function of the excitation frequency ω_L , often tracks closely with the absorption spectrum but is not identical to it and may, in some cases, have a very different

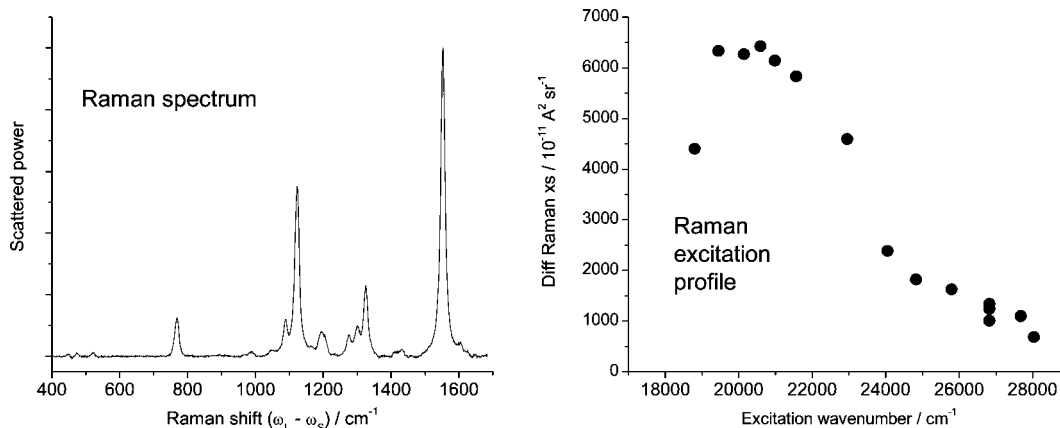


Figure 4. Raman spectrum (left), which is a plot of the Raman scattered power as a function of Raman shift at a fixed excitation frequency ω_L . The integrated area under each peak is proportional to the Raman cross-section for the corresponding $|i\rangle$ to $|f\rangle$ transition. Raman excitation profile (right), which is a plot of the cross-section for a single $|i\rangle$ to $|f\rangle$ Raman transition as a function of excitation frequency.

shape. Figure 4 compares a resonance Raman spectrum with an excitation profile.

This review focuses on spontaneous resonance Raman and hyper-Raman scattering originating in ground electronic states; however, several related forms of Raman spectroscopy should also be mentioned:

- In time-resolved or transient Raman spectroscopy, a short “pump” laser pulse is used to promote an ensemble of molecules to an excited electronic state or to produce a short-lived photoproduct, and a subsequent “probe” pulse then excites the spontaneous Raman spectrum of the transient species.^{8–17} Transient Raman scattering has been carried out on a wide variety of systems with laser pulses that vary from nanoseconds to subpicosecond in duration, although very short pulses, because of their necessarily broad spectral bandwidth, provide poorly resolved Raman spectra. The desired transient species may be observed without much interference from the parent species if the probe pulse is on resonance with an electronic transition that is unique to the species of interest. This is a very useful technique for obtaining vibrational spectra of comparatively short-lived or nonequilibrium systems.

- Coherent anti-Stokes and coherent Stokes Raman scattering (CARS and CSRS, respectively) and a variety of related techniques^{18–21} are nonlinear spectroscopies in which multiple incident excitation beams produce a signal in the form of a laserlike, directional beam that arises from the coherent polarization of molecules throughout the illuminated volume. These processes involve intermediate vibrational coherences and therefore exhibit Raman resonances and can be carried out under electronically resonant conditions. The directional nature of the signal simplifies separation of the Raman signal from the spontaneous fluorescence which is often a major source of interference in resonance Raman. However, in coherent Raman processes all contributions to the signal at a given frequency, both vibrationally resonant and nonresonant, add at the level of the electric field amplitude rather than the intensity. These multiple contributions to the signals can therefore exhibit interferences leading to complicated, hard to analyze line shapes, and the spectrum of a mixture (e.g., solute plus solvent) is not just the sum of the individual component spectra.

- In impulsive stimulated Raman scattering,^{22–25} one or more pump laser pulses that are temporally shorter than vibrational periods generate a coherence between vibrational levels of either the ground state or an excited electronic state, and the transmission of a variably delayed probe pulse is detected. The probe transmission is modulated at frequencies that correspond to the

vibrational coherences created by the pump, and Fourier transformation or similar analysis of the time-dependent signal yields the vibrational frequency spectrum. When carried out under electronically resonant conditions, the amplitudes of each of the frequency components yield information about the Franck–Condon activity of each mode in the resonant electronic transition, similar to the information contained in spontaneous resonance Raman intensities. The analysis can be complicated by interfering contributions from ground-state coherences, which modulate the absorption, and excited-state coherences, which modulate the stimulated emission. It can also observe only those vibrations that have periods longer than the pulse durations. This technique is therefore most useful for probing the Franck–Condon activity of very low-frequency vibrations that are typically difficult to observe in spontaneous Raman because of the strong nearby elastic (Rayleigh) scattering.

- Surface enhanced Raman scattering (SERS) refers to the large enhancement in the Raman scattering intensity when the molecule of interest is adsorbed to the surface of a nanostructured metal, most notably silver or gold.^{26–32} It can occur either with or without molecular electronic resonance. The phenomenology and theory of SERS have been studied extensively because the huge signal enhancements (typically 10^4 to 10^6 , much greater for molecules in special “hot spots”) make the technique tremendously useful for ultrasensitive analytical applications. “Chemical” mechanisms usually involving the formation of molecule–metal charge-transfer states may contribute to SERS, but the major contribution in most cases appears to be the “electromagnetic” mechanism that results from coupling of the incident and scattered fields to surface plasmons (collective excitations of the conduction electrons) of the metal. It is usually described classically as an enhancement of the local electric fields at the surface of the metal, although a quantum mechanical analog has also been presented.³³ SERS is typically used as a ground-state vibrational spectroscopy, although the influence of excited-electronic-state properties on electronically resonant SERS has been addressed in a few papers.^{33–37}

Raman scattering involves destruction of one photon from the incident electromagnetic field coupled to creation of a photon at the scattered frequency. Analogous processes that involve more than one photon in either or both steps are also possible. The best-known such process is hyper-Raman scattering, in which two (usually identical) photons are destroyed and one scattered photon is created.^{38,39} In Stokes vibrational hyper-Raman, the difference ($2\omega_L - \omega_S$) must match a ground-state vibrational frequency as ($\omega_L - \omega_S$) does in ordinary Stokes

vibrational Raman, and excitation with a red or near-IR laser creates scattering in the near-UV to green. In hyper-Raman the scattered power is proportional to the square of the incident intensity, and pulsed laser excitation is usually required to provide the necessary peak intensity (although see ref 40). Hyper-Raman scattering has been known since the early days of pulsed lasers but is rarely performed in liquid solutions, mainly because of the usual weakness of the effect; other nonlinear processes such as self-focusing, continuum generation, and/or dielectric breakdown of the solvent often interfere with or dominate the desired hyper-Raman scattering.³⁹ However, we and others have shown that in molecules that are both highly polar and highly polarizable, electronically resonant hyper-Raman scattering can be reasonably strong and a useful spectroscopic tool.^{41–53} It provides information about the Franck–Condon active vibrations coupled to transitions that are both one- and two-photon allowed, as discussed further below.

This review approaches resonance Raman and resonance hyper-Raman scattering as vibronic spectroscopies and addresses what they reveal about the structure and dynamics of excited electronic states of molecules in liquid solution. The better established technique of resonance Raman is discussed first, followed by a much briefer section on resonance hyper-Raman. Each section starts with a brief historical retrospective on the development of the technique from both experimental and theoretical/interpretive perspectives. The current state of the art is then discussed, again with reference to both experiment and theory, and a few specific examples are shown. Finally, an attempt is made to predict the future of each spectroscopy: how will it be done experimentally, on what systems will it be performed and for what reasons, and how will the results be used?

Resonance Raman Spectroscopy

Historical Development: Experiment. The Raman effect owes its name to C. V. Raman, who (with K. S. Krishnan) first reported the effect in 1928^{54,55} and later won a Nobel Prize for correctly describing it. For the first 40–50 years after its discovery, Raman scattering remained a technique of marginal utility mainly because of the lack of intense, narrow-bandwidth light sources available for excitation. (Remarkably, C. V. Raman originally observed the effect by using bandwidth-narrowed sunlight as an excitation source.) Excitation was typically provided by resonance lines from arc lamps, which are spectrally narrow but not easily collimated or focused. To compensate for the relatively low intensity of the excitation source, detection was usually performed by dispersing a large portion of the scattered spectrum onto a photographic plate. This allowed the entire scattered spectrum to be integrated over a long period of time to compensate for its weakness, but photographic plates were cumbersome to use and lacked both sensitivity and dynamic range. Despite these limitations, Raman spectra of an impressively large number of compounds were characterized in the “pre-laser” days.⁵⁶

The enabling technology that turned Raman scattering into a routinely useful laboratory technique was the laser, which provided an intense source of monochromatic light that could be focused to a small spot. With the higher incident light intensity, the scattering was strong enough that the scattered light could be scanned, one frequency element at a time, across a single-element detector, typically a cooled photomultiplier tube coupled to photon counting electronics. This enabled spectra to be obtained at higher resolution with better signal-to-noise ratio and greater dynamic range than was possible with

photographic plates, and also made possible interfacing of the detection electronics to the microprocessors and primitive computers that began entering research laboratories in the 1970s. From the 1970s to the present, continued improvements in the ease of use, stability, compactness, and frequency tunability of commercial lasers have allowed continued advances in Raman spectroscopy.

The other major advance in Raman instrumentation was the development of high-quality multielement array detectors, particularly charge-coupled device (CCD) detectors. CCDs are now the detector of choice for nearly all Raman experiments except those that require detection in the far-UV or the true IR region. A cooled CCD combines the multichannel advantage (the ability to integrate signal in hundreds to thousands of frequency elements simultaneously) with negligible dark current and quantum efficiencies that equal or surpass those of photomultipliers. Additionally, CCDs are very difficult to damage by accidental exposure to high light levels, unlike photomultipliers. Thus instrumentation for Raman detection has come full circle, from intrinsically multichannel photographic plates to single-channel photomultipliers and now back to multichannel array detectors.

Historical Development: Theory. The theory of Raman scattering from isolated molecules was first developed by Kramers and Heisenberg in 1925⁵⁷ and independently by Dirac in 1927⁵⁸ and is generally referred to as the Kramers–Heisenberg–Dirac (KHD) equation. Both papers used second-order time-dependent perturbation theory to derive the rate at which a system makes transitions from the material state $|i\rangle$ to state $|f\rangle$ while the quantized radiation field loses one photon from the mode having frequency and polarization (ω_L, \mathbf{e}_L) and gains one photon into the initially unoccupied mode at (ω_S, \mathbf{e}_S) . The requirement of overall conservation of energy, $\hbar(\omega_L - \omega_S) = E_f - E_i$, falls out naturally from taking the $t \rightarrow \infty$ limit. The system proceeds from the initial to the final state through a superposition of all intermediate states that differ from both the initial and the final state by only one photon. The result is the equation for the Raman polarizability given in eq 1, where for isolated molecules the line width should be taken as that arising from purely radiative decay processes.

Direct evaluation of eq 1 is daunting because, in principle, all electric dipole allowed intermediate states $|v\rangle$ (all vibration–rotation levels of all electronic states) contribute to the sum. Arguments based on classical polarizability theory and molecular symmetry are useful for predicting which vibrational modes are Raman active but cannot explain the incident frequency dependence of Raman intensities or quantitative resonance effects. Although many others made useful contributions, the modern theory of resonance Raman intensities is based largely on the work of Albrecht and collaborators in the 1960s.^{59–61} They treated Raman scattering as a vibronic spectroscopy and showed how Raman intensity could arise from several different mechanisms. “A-term” scattering results from the Franck–Condon activity of totally symmetric vibrations in one or more electronic states that serve as intermediate states in the scattering process. A-term scattering is often expected to dominate when the excitation frequency is on or near resonance with a strongly allowed electronic transition, but its intensity drops off quickly with detuning from resonance. “B-term” and “C-term” scattering arise from the vibrational coordinate dependence of the electronic transition moments and can contribute to Raman intensity in both totally symmetric and nontotally symmetric vibrations. These are the dominant sources of Raman intensity when the excitation is far from resonance

or near resonance with a transition that is electronically forbidden but vibronically allowed.

In the simplest situation where the excitation frequency is very near or on resonance with a single electronic state that is nondegenerate and strongly allowed, the A -term is expected to dominate, only one element of the Raman polarizability tensor is important, and the second term in eq 1 may be neglected because its denominator can never be small. Equation 1 then becomes

$$\alpha_{I \rightarrow F}(\omega_L, \omega_S) = |M_{eg}|^2 \sum_V \left\{ \frac{\langle F|V\rangle\langle VI\rangle}{\omega_L - \omega_{eV,gl} + i\tilde{\Gamma}_{eV,gl}} \right\} \quad (5)$$

$|I\rangle$ and $|F\rangle$ are vibrational levels of the ground electronic state $|g\rangle$, and $|V\rangle$ is a vibrational level of the resonant electronic state $|e\rangle$; M_{eg} is the purely electronic transition moment. Neglect of the vibrational coordinate dependence of the transition moment corresponds to the Condon approximation, whereas non-Condon contributions may be taken into account to low order by including the B term. Equation 5 is still very difficult to evaluate directly, as it involves knowledge of the vibrational overlap integrals between the initial and final ground-state vibrational wave functions and all of the $3N - 6$ dimensional excited-state vibrational wave functions for an N -atom molecule. Even if the simplest possible assumptions are made about the form of these wave functions (e.g., separable harmonic oscillators), the sheer number of states that must be included in the sum severely taxed the capabilities of the computers available to most experimentalists in the 1970s and beyond. A second difficulty involves the line width parameter, $\sim\Gamma_{eV,gl}$. Early efforts to measure and model resonance Raman excitation profiles from large, visible-absorbing conjugated molecules in solution, using a small number of intermediate vibronic levels, required very large line widths on the order of 1000 cm^{-1} . Such large line widths could not sensibly be interpreted as purely radiative in origin, but it was not clear whether the discrepancy was due to vibronic congestion (not enough $|V\rangle$ levels were being included), inhomogeneous broadening (different molecules in slightly different local environments in the liquid having slightly different transition frequencies), or other mechanisms.

The question of the appropriate line width and line broadening function to use in resonance Raman calculations leads directly to the more general issue of how to describe a spectroscopically active “system” interacting with a “bath” which does not, by itself, contribute directly to the spectroscopic signal of interest. This question is reviewed in detail from both an experimental and a theoretical perspective in ref 62 and will be summarized only briefly here. It is intimately related to the distinction between resonance Raman scattering, a coupled two-photon process, and laser-induced fluorescence, a result of sequential absorption and emission steps.^{63–68} If there is no bath—that is, all of the relevant material degrees of freedom are encompassed by the eigenstates $|i\rangle$, $|f\rangle$, and $|v\rangle$ in eq 1—then there is, in principle, no distinction between resonance Raman and laser-induced fluorescence under steady-state monochromatic excitation. There is only one process, “resonance secondary emission”, described by second-order time-dependent perturbation theory in the weak field limit. However, most resonance Raman experiments are performed on molecules dispersed in a solid matrix or dissolved in a liquid solvent, often at or near room temperature. Under these conditions the total emission spectrum usually exhibits two clearly distinguishable components, a “fluorescence” component with a breadth comparable to that of the absorption spectrum whose position and shape are entirely or nearly independent of the excitation wavelength and a

“Raman” component with line widths comparable to those of vibrational infrared spectra and positions that track with the exciting laser frequency. To describe the fluorescence component theoretically, it is necessary to adopt a density matrix treatment to describe the system–bath interactions. This was developed in a large number of theoretical papers during the 1960s through 1980s and demonstrated in experiments at low temperatures where the gradual conversion from one type of emission to the other can be observed. These studies led to the understanding that when the spectroscopically active molecule is interacting with an environment, the line width in eq 1 should be understood as a total dephasing width that, at least in a room-temperature liquid, is generally much larger than the radiative line width. More sophisticated treatments, however, also pointed out that the dephasing induced by solvent–solute interactions is not exponential at short times and the resulting line shape is not purely Lorentzian as implied by eq 1. Furthermore, these effects can even come into play in gas-phase experiments, as parts of a molecule that do not directly participate in the electronic excitation can serve as a stochastic bath for the eigenstates of the chromophoric part of the molecule.

The issue of “homogeneous” versus “inhomogeneous” electronic spectral broadening is also one that was largely settled, at least theoretically, in the 1970s and 1980s. In spontaneous Raman scattering, each molecule scatters independently; the contributions from different molecules add at the level of the scattered power or Raman cross-section (eqs 3 and 4), not at the level of the electric field or Raman polarizability (eq 1). If the overall electronic transition width of an ensemble of molecules arises mainly from the fact that different molecules sit in slightly different local environments and thus have slightly different perturbations to their transition frequencies, this must be included in Raman intensity calculations by averaging over a distribution of cross-sections for molecules with slightly different resonant frequencies. If, on the other hand, the observed electronic width implies a large radiative or solvent-induced dephasing width for each molecule, that width contributes to the Raman polarizability and acts to damp the resonance Raman intensity. The different roles played by homogeneous and inhomogeneous broadening in resonance Raman scattering were pointed out fairly early and absolute Raman cross-section measurements were used to distinguish between the two types of broadening.^{4,69,70} However, such a separation sweeps under the rug the fact that most environments generate perturbations to the molecular transition frequencies that fluctuate on a wide range of time scales, so there is no clear separation between homogeneous and inhomogeneous broadening.⁶² Mukamel and co-workers considered this problem quantitatively in several important papers that demonstrated that there is not, in general, any clean separation between solvent-induced broadening mechanisms that act at the Raman polarizability level and those that act at the cross-section level. However, they also showed that, under most conditions for molecules in room-temperature liquid solutions, the time scales of the various processes are such that the part of the emission that is spectroscopically identifiable as Raman scattering can still be described approximately as the modulus squared of a KHD-like polarizability; however, the simple Lorentzian line shape of eq 1 is usually not a good approximation, and a much more complicated formula that arises from a dephasing function that is Gaussian at short times and exponential at longer times is required.^{67,68}

The other major theoretical development that enabled practical computational simulations of resonance Raman scattering for large molecules was the “time-dependent” theory of resonance

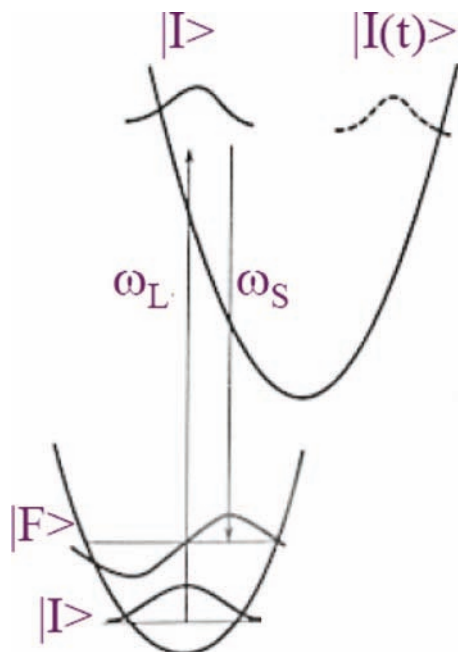


Figure 5. Interpretation of the time-domain formulation of resonance Raman scattering. The initial vibrational wave function $|I\rangle$ is sent to the excited-state surface by the incident photon of frequency ω_L and propagates under the influence of the excited-state vibrational Hamiltonian. The Fourier transform of the overlap between this moving wavepacket, $|I(t)\rangle$, and itself at time zero, $|I\rangle$, gives the optical absorption spectrum. The absolute square of the half-Fourier transform of the overlap between $|I(t)\rangle$ and the final state in the Raman process, $|F\rangle$, gives the Raman excitation profile.

Raman initially developed by Heller in 1979.^{71–74} Though the derivation of the KHD equation (eq 1) uses time-dependent perturbation theory, the equation describes a steady-state transition rate under continuous monochromatic excitation—i.e., the experimental observable is not time-dependent—and the resulting time propagators have been removed by inserting a complete sum over states, allowing all time integrals to be done analytically. The resulting eq 1, however, contains an infinite sum over intermediate states that must be evaluated numerically. Heller demonstrated, both by direct first-principles derivation⁷¹ and later starting from the KHD equation,^{72,73} that keeping the equation in its time propagator form could be highly beneficial from both an intuitive and a computational point of view. He pointed out that if the resonant electronic transition is very broad, either because it is short-lived or because it has a high density of allowed vibronic transitions (Heller considered only isolated molecules), the individual eigenstates $\{|v\rangle\}$ in eq 1 are not resolved and it cannot be necessary to know each individual eigenvalue and matrix element. Rather, resonance Raman scattering (and optical absorption) can be described as the time integral of the overlap between a moving wavepacket, which is the initial ground-state vibrational wave function propagated on the excited-state potential energy surface, with the final state in the Raman process (or, for absorption, with itself at time zero). A physical interpretation is shown in Figure 5. Because often only short-time dynamics are important, it is not necessary to know the entire excited-state potential energy surface required to calculate all the vibrational eigenstates; only the small piece of that surface near the ground-state geometry is needed. This is particularly useful for handling excited states that are dissociative⁷⁵ or highly anharmonic.

The time-dependent theory also turned out to be a huge computational advantage for handling large molecules that

undergo only small geometry changes along each normal mode and can be reasonably well approximated as separable harmonic oscillators.^{73,74} In such cases, each vibronic eigenstate is a product of the wave functions in each of the $3N - 6$ vibrational degrees of freedom and the vibronic structure of the electronic transition is a convolution of the Franck–Condon factors in each vibrational mode. The time-domain analog of eq 5 is⁴

$$\alpha_{I \rightarrow F}(\omega_L, \omega_S) = |M_{eg}|^2 i \int_0^\infty dt \exp[i(\omega_L + \omega_S)t - \Gamma t] \langle F | I(t) \rangle \quad (6)$$

where $|I(t)\rangle = e^{-iHt/\hbar}|I\rangle$ is the initial vibrational wave function propagated by the excited-state vibrational Hamiltonian H , and the line width Γ is assumed constant for all vibrational levels of the resonant electronic state. For separable harmonic modes the multimode overlap integral is a product of single-mode overlaps, $\langle F | I(t) \rangle = \prod_m \langle f_m | i_m(t) \rangle$. If there are, e.g., 30 important vibrational modes and each mode has four Franck–Condon active states, 4^{30} eigenstates will contribute to the sum in eq 5 but eq 6 requires only multiplying 30 overlap functions at each time point and then performing a numerical Fourier transform, a much simpler calculation.

Modern Implementation: Experiment. Resonance Raman spectroscopy is performed on gases, liquids, solids, and a wide variety of complex materials, and the mechanical and optical setups employed for excitation and collection are correspondingly diverse. Essentially all Raman experiments are now performed with laser excitation. For several reasons (ground-state depletion, photochemical damage, undesired nonlinear responses, line width of the laser source) resonance Raman experiments that do not require time resolution are ideally performed with continuous-wave (cw) excitation, but pulsed lasers are often used to take advantage of the broad wavelength tunability afforded by nonlinear wave-mixing processes. Ion and dye lasers are still simple, versatile cw sources for tunable visible excitation, although cw dye lasers have nearly disappeared from the commercial laser market. Diode lasers are increasingly popular inexpensive sources for cw excitation in the red and near-IR, as are frequency doubled cw Nd lasers for green excitation. Pulsed Nd:YAG lasers, together with harmonic generation and/or stimulated Raman shifting, are well established pulsed excitation sources particularly for UV excited Raman work. Ti:sapphire lasers, the mainstay of modern ultrafast laser science, are also widely used as high repetition rate sources in resonance Raman spectroscopy: the near-IR fundamental, near-UV to green second harmonic, and UV third harmonic can be used directly, and parametric wave mixing provides greater tunability.

The vast majority of modern Raman instruments utilize a grating spectrometer to separate the scattered wavelengths and a multichannel detector, usually a charge-coupled-device (CCD) with thermoelectric or liquid nitrogen cooling. Different schemes are used for removing interference from the usually strong scattered laser light. With some materials and sampling geometries it is possible to obtain good quality resonance Raman spectra using a single spectrograph with no additional filtering, particularly if only relatively large Raman shifts are of interest. Holographic notch filters can provide very good laser line rejection together with high transmission for the Raman shifted light,⁷⁶ but each relatively expensive filter normally works at only a single laser wavelength and Raman spectra can be obtained to within only a few hundred cm^{-1} of the laser line. When broadly tunable excitation is required and/or small Raman shifts need to be observed, the instrument of choice is normally

a triple spectrograph consisting of a subtractive double monochromator as a prefilter stage coupled to a single spectrograph. Drawbacks to this solution are the large size and complexity of the detection apparatus and the low throughput because of the large number of optical elements involved.

A completely different approach to detection, which has become very popular for nonresonant Raman spectroscopy, is Fourier transform Raman (FT-Raman).^{77,78} In FT-Raman, the different scattered wavelengths are not separated; rather, all of the scattered light, after filtering out the strong laser scatter, is directed into an interferometer and the light intensity impinging on a single detector is measured as a function of the path length difference. The frequency spectrum of the scattered light is obtained from a Fourier transform of this interferogram. A Fourier transform instrument can provide a higher signal-to-noise ratio than a dispersive instrument when the detected light is in the near-infrared region, where detectors are generally noisy, and can also have advantages in spectral resolution and frequency precision. Most FT-Raman instruments utilize excitation from a compact, continuous-wave Nd:YAG laser at 1064 nm. This wavelength falls to the red of electronic absorption bands of most molecules, making FT-Raman systems ideal for routine characterization of samples without fluorescence interference. Fourier transform detection is rarely used in resonance Raman spectroscopy because of the shorter excitation wavelengths usually required, but resonance Raman in the near-IR may become more common with the increasing interest in far-red and near-IR absorbing molecules for various materials applications.

In resonance Raman experiments, unlike ordinary Raman, one is usually interested in not only the frequencies of the Raman lines but also their quantitative intensities, at least relative intensities and often absolute Raman cross-sections. In either case, it is necessary to perform intensity corrections on the measured Raman spectra.^{4,6} There are a number of experimental factors that cause the detection efficiency to vary across the wavelength range of a Raman spectrum. These include wavelength-dependent reabsorption of the scattered laser light by the absorbing sample, the wavelength-dependent throughput of all of the optics in the spectrograph and detection system (particularly the diffraction efficiency of the grating(s)), and the wavelength-dependent quantum efficiency of the detector. The reabsorption correction can be calculated from knowledge of the sample's absorption spectrum and the excitation and detection geometry, and/or by comparing the intensities of solvent Raman bands in the pure solvent and in the absorbing solution. Collection and detection efficiency corrections are normally made by acquiring a spectrum of a calibrated continuous lamp with a known emission spectrum, although differences in the geometry of the lamp and the Raman scattering source can cause complications. An additional problem, particularly severe in UV-excited Raman spectroscopy, is the wavelength-dependent focal length of the collection optics, which causes different Raman shifts to be transmitted through the spectrograph entrance slit with unequal efficiencies. For this reason quantitative resonance Raman measurements, particularly in the UV, are often made using reflective collection optics (Cassegrain telescope or ellipsoidal mirror)^{79–81} rather than transmissive lenses. Reflective optics can be more complicated to align, have a smaller effective collection angle, and/or do not provide as tight a focus for extended scattering sources as lenses, but the wavelength dependence of the efficiency is usually gently varying and straightforward to correct.

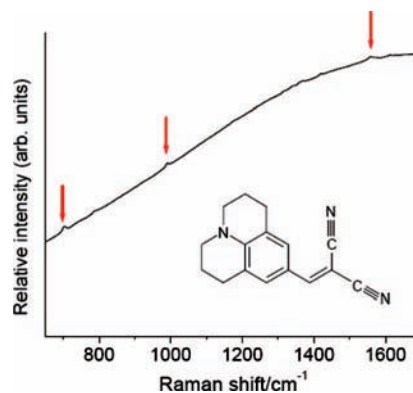


Figure 6. Spontaneous emission spectrum of julolidinemalononitrile showing small Raman peaks (red arrows) superimposed on a large fluorescence background. Subtraction of the background (fit to a low-order polynomial) leaves resonance Raman spectra such as those shown in Figure 8 below.

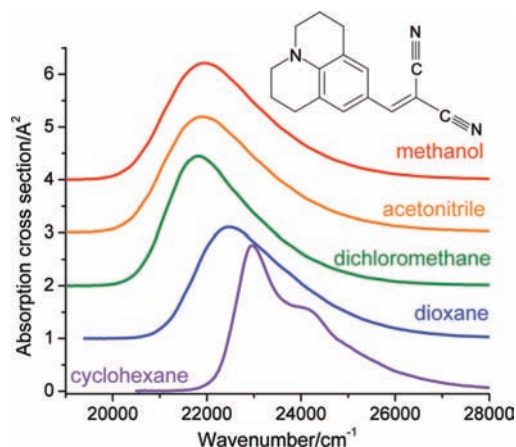


Figure 7. Absorption spectra of JM in five solvents. Spectra are displaced vertically for display. Data from ref 103.

Most molecules, following excitation within an allowed electronic absorption band, emit much more light as fluorescence than as Raman scattering. Roughly speaking (refer to discussion above under Theory), fluorescence is stronger than Raman scattering by the ratio of the excited-state population lifetime to the electronic dephasing time, a ratio that is typically 10^3 to 10^6 or larger. Usually the fluorescence is peaked at longer wavelengths than the Raman scattering because much of the fluorescence emission is preceded by vibrational relaxation and/or solvent reorganization. Nevertheless, Raman spectra are usually accompanied by a broad underlying fluorescence background, as shown in Figure 6. Even though the fluorescence is usually very broad and readily distinguishable from the Raman scattering, its presence can severely degrade the signal-to-noise ratio of the Raman spectrum because of the large photon shot noise accompanying the fluorescence signal. The shot noise is given by $N^{1/2}$ where N is the number of detected photons. If a Raman line has 100 detected photons at the peak and there is no fluorescence background, the shot noise is 10 and the signal-to-noise ratio at the peak is 10. If, however, the same 100 photon counts of Raman scattering lie atop a fluorescence background of 10^6 counts, the shot noise at the Raman peak is now 1000 and the signal-to-noise ratio at the peak of the Raman line is only 0.1. This explains why it is nearly impossible to obtain useful spontaneous resonance Raman spectra of highly fluorescent molecules unless the excitation wavelength is chosen such that the Raman spectrum does not fall in a region of strong fluorescence. Pulsed laser excitation can be coupled with gated

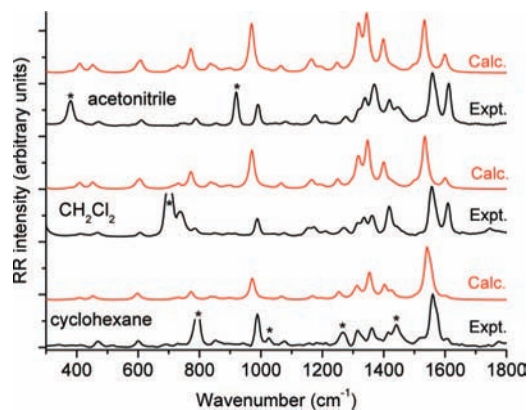


Figure 8. Black: experimental resonance Raman spectra of JM in three solvents at 424 nm excitation. Spectra are displaced vertically for display and asterisks label solvent bands. Experimental procedures are described in ref 103 Red: corresponding spectra calculated using time-dependent density functional theory and the “short-time” approximation as described in ref 94.

detection to exclude some of the longer-lived fluorescence, but such approaches have not achieved widespread use.^{82–85} Normally, the fluorescence background is considered uninteresting, so it is removed by fitting a low-order polynomial or some other smooth curve to the background and subtracting it, leaving behind the “pure” Raman spectrum as shown in Figure 8. Note that any corrections for the wavelength- or pixel-dependent detection efficiency must be made prior to subtracting the fluorescence, and they must be made carefully when the Raman lines of interest are only a few percent of the total signal detected. It is also easy to introduce distortions into the Raman spectra by subtracting a “background” that has more structure than the true fluorescence. Once the necessary intensity corrections have been made and the fluorescence background subtracted, the integrated areas of the Raman lines must be determined, generally by fitting the whole spectrum or regions of the spectrum to a sum of peaks of some assumed functional form and, often, a small residual background. It is the peak areas that are proportional to the quantities of interest, the differential Raman cross sections.

Absolute cross sections for resonance Raman scattering are usually measured relative to a known nonresonant internal standard, often one of the solvent Raman bands. For experiments in water, whose Raman lines are very broad, an added internal standard such as sulfate ion is often used. The absolute cross section of a resonance Raman line of interest can then be calculated from the ratios of the integrated intensities of the standard and sample Raman bands, after intensity correction as described above, and the concentrations of sample and standard. Most reported absolute cross-section “standards” have actually been determined relative to other standards; very few direct, primary measurements of absolute cross-sections have been reported.^{86–89} These measurements are difficult because the large difference between incident laser and Raman scattered powers (10^6 to 10^{10}) requires calibration of the detector over a wide dynamic range, and because of the difficulty in determining accurately the solid angle over which the Raman scattered light is collected. Typically direct measurements are made at a few excitation wavelengths and then a theoretically justifiable function such as a preresonant “A-term” is used to interpolate, and in some cases extrapolate, to wavelengths not directly measured. As the wavelength dependence of the cross-section for far off-resonance scattering is quite gentle, interpolation is probably well justified; however, the accuracy of the primary

data points is often questionable. The lack of reliable primary Raman cross-section standards is one of the main limitations to the accurate determination of absolute cross-sections for resonance Raman scattering.

Modern Implementation: Theory. Resonance Raman intensities are sensitive to the difference between the ground-state and resonant excited-state potential energy surface along specific vibrational modes, and therefore to the change in molecular geometry upon electronic excitation. As outlined above, if the potential energy surfaces are known, it is more or less straightforward (depending on the approximations employed, and additional contributing factors such as the magnitude and nature of the electronic transition line widths) to calculate the expected resonance Raman intensities by utilizing eqs 2–4 plus eq 5 or 6. However, as with many other “inverse” spectroscopic problems, the potential energy surfaces cannot be determined from the measured Raman intensities through any straightforward analytical procedure even at the simplest level of approximation.

One way to address this quandary is to describe the molecular system with a parametrized model and attempt to determine empirically the parameters that reproduce the experimental resonance Raman data. The parameters minimally required to calculate resonance Raman intensities are the ground- and excited-state vibrational frequencies for each normal mode, the differences between ground- and excited-state potential minima in each mode, the magnitudes and functional forms of the homogeneous and any inhomogeneous broadening, the electronic zero-zero energy, and the electronic oscillator strength. Other factors such as Duschinsky rotation (mixing of the ground-state normal coordinates to form the excited-state normal coordinates), vibrational anharmonicities, vibrational coordinate dependence of the electronic transition moment, multiple electronic states, and thermal population of initial states other than the ground state⁹⁰ may also be included. One starts by making educated guesses for the parameters, calculates the resonance Raman intensities (as well as the optical absorption spectrum, which depends on the same parameters), compares them to experiment, adjusts the parameters, and continues with an iterative adjust-and-calculate procedure until the calculated and experimental spectra agree as closely as possible.⁴ Goodness of fit may be ascertained either “by eye” or through a quantitative criterion such as minimized root-mean-squared error, although implementation of the latter is complicated by the incommensurate nature of optical absorption and Raman intensity data. If the final best fit is judged inadequate, the data are subject to further scrutiny and/or one or more assumptions of the model are changed. This procedure can be very time-consuming even for an experienced operator who has a good physical sense of how a particular change in a parameter will affect the spectra. The effects of the different parameters are strongly coupled to one another and it is often difficult to foresee how a change in a parameter describing one mode will affect the Raman profiles for other modes. Furthermore, there is no way to be certain that one has found the best set of parameters or to know whether the best-fit parameter set is unique. Recent progress in automating the refinement process makes the procedure much less time-intensive for the human involved, more reliable, and free of operator bias.^{91–93} However, questions of the uniqueness of the solution and adequacy of the chosen model remain.

An alternative approach is to generate the molecular parameters in a completely independent manner, calculate the resulting resonance Raman intensities, and use the agreement (or lack

thereof) between experimental and calculated data to evaluate the accuracy of the calculated parameters. Until recently, electronic structure calculations of molecular excited-state potential surfaces for medium sized molecules were not good enough to achieve more than crude qualitative agreement with experiment, but there have recently been some impressive successes including remarkably accurate calculations of solvent effects on resonance Raman spectra.⁹⁴ In calculations on medium-sized to large molecules harmonic approximations usually have to be made at least for most modes,^{95–97} whereas for small molecules resonance Raman intensities can be calculated through wavepacket propagation on the full anharmonic potential surface.^{98,99} It seems clear that as computational electronic structure methods become increasingly accurate and powerful, such *ab initio* resonance Raman intensity calculations will become increasingly useful both for interpreting experimental results and for guiding further improvements in electronic structure methods.

Examples. Resonance Raman spectroscopy is a powerful probe of solvent effects on molecular structure because the experiments can be performed in a wide variety of solvents or other molecular environments. “Push–pull” conjugated molecules,^{42,94,100–106} which consist of electron donating and electron accepting groups connected through a π -conjugated linker, are particularly interesting subjects for solvent effect studies. They are simultaneously quite polar and highly polarizable, and many of them have strong, low-lying electronic transitions that have a high degree of intramolecular charge-transfer character. Many of these molecules also have strong nonlinear optical responses to red or near-IR radiation. As most nonlinear optical applications require a specific condensed-phase environment, it is important for practical reasons to understand how the molecular properties vary with environment. Experimental studies of solvent effects on ground- and excited-state structures also provide a challenging test for computational methods that incorporate models for the solvent environment into electronic structure calculations.^{53,100,103,104,107–109}

Figure 7 shows the solvent-dependent absorption spectra of one such push–pull molecule, julolidinemalononitrile (JM), whose resonance Raman and fluorescence spectrum was shown in Figure 6. The absorption spectrum broadens and red-shifts as the solvent polarity or polarizability increases. Raman spectra obtained using excitation throughout this band show not only the expected dependence of the Raman intensity on excitation wavelength on tuning through the absorption band but also some significant changes in the relative intensities of different lines in different solvents.¹⁰³ Figure 8 (black lines) shows spectra in a nonpolar solvent (cyclohexane), a moderately polar and quite polarizable solvent (dichloromethane), and a highly polar solvent (acetonitrile). Although the positions of the lines vary by a maximum of ~ 5 cm^{-1} among solvents, indicating that the ground-state vibrational frequencies are only slightly solvent sensitive, the intensities of some lines show strong variations. For example, the line near 1612 cm^{-1} , which is almost as strong as the ~ 1558 cm^{-1} line in acetonitrile, is nearly undetectable in cyclohexane.

Guthmüller and Champagne have calculated these solvent-dependent absorption and resonance Raman spectra using time-dependent density functional theory coupled with the polarizable continuum model for the solvent.⁹⁴ They tested hybrid exchange–correlation functionals containing various fractions of exact Hartree–Fock exchange and found that the best results were obtained with about 35% of exact exchange included in the exchange–correlation functional.⁹⁴ Figure 8 (red curves) shows

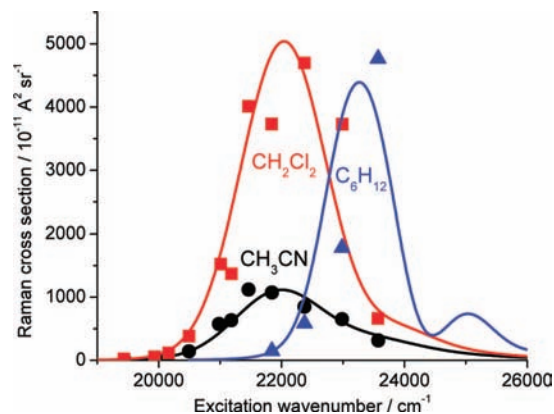


Figure 9. Resonance Raman excitation profiles for the 990 cm^{-1} mode of JM in the three solvents indicated. Points represent experimental data from ref 103 and lines are the simulated profiles using the empirical modeling parameters of ref 103.

that the solvent dependence of the ~ 1612 cm^{-1} line is reproduced quite well by the calculations, as are the qualitative intensity patterns the remainder of the spectra. This demonstrates the utility of experimental data of this type in refining computational methodologies. The calculations also provide additional details about the solvent dependence of both the ground-state normal modes and the excited-state potential energy surface, not evident from analysis of the experimental data alone, that aid in more fully interpreting the experimental results.

In addition to the solvent-dependent relative intensities of the resonance Raman lines, the absolute Raman cross-sections also vary considerably among solvents. A reduction in the absolute cross-section for a given Raman line may arise from either a reduction in the excited-state geometry change along that mode or an increase in the homogeneous electronic broadening. Self-consistent modeling of the absorption spectra and Raman profiles is needed to untangle the two effects. When this modeling is carried out, it is found that some modes (e.g., the 1612 cm^{-1}) have strongly solvent-dependent excited-state displacements (Δ) whereas in other modes the Δ is nearly the same in all solvents examined. Figure 9 compares the resonance Raman excitation profiles for a mode of the latter type, the 990 cm^{-1} line, in three solvents. Although Δ varies by only about 10% across this set of solvents, the peak cross-section varies by about a factor of 4. This is mainly a consequence of changes in the homogeneous broadening; the solvent reorganization energy obtained from these simulations is about three times larger in acetonitrile than in the other two solvents. The unusually rapid electronic dephasing in acetonitrile, compared with other solvents, is probably connected to the large and rapid “inertial” component of the solvent reorganization in this solvent.¹¹⁰

The electronic transitions of push–pull molecules such as JM typically involve a large change in dipole moment. At the extreme end of this spectrum are electronic transitions of ground-state charge-transfer complexes, in which noncovalently bonded electron donor and electron acceptor moieties undergo intermolecular electron transfer upon absorbing a photon, $D^+ \xrightarrow{h\nu} A^-$. Analysis of the Raman intensities obtained by exciting on resonance with such a charge-transfer transition allows determination of the mode-specific vibrational reorganization energies that accompany the electron-transfer process.^{5,111–123} These reorganization energies are an important factor in determining the rates of analogous nonphotoinduced electron-transfer processes which are important in natural photosynthetic systems, artificial solar energy harvesting systems, photography, and xerography, to name a few.

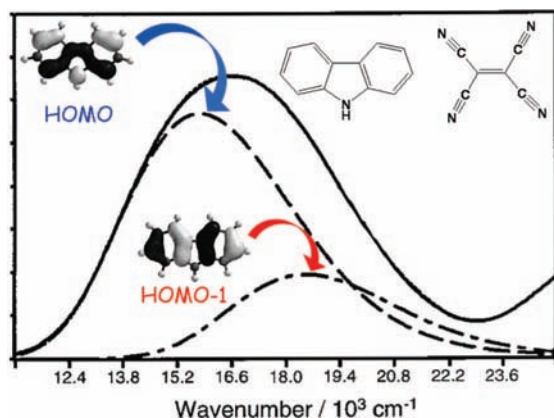


Figure 10. Optical absorption spectrum of the 1:1 charge-transfer complex of carbazole with tetracyanoethylene (solid curve) and its resolution into two separate transitions (HOMO of carbazole to LUMO of TCNE, dashed; HOMO-1 of carbazole to LUMO of TCNE, dot-dashed). Data from ref 120.

Figure 10 illustrates the absorption spectrum of the ground-state charge-transfer complex between carbazole (electron donor) and tetracyanoethylene (TCNE; electron acceptor). A 1:1 carbazole-TCNE complex forms spontaneously with a large equilibrium constant in an appropriate solvent. Although neither carbazole nor TCNE alone absorbs in the visible, their charge-transfer complex has a broad absorption band spanning the visible spectrum. This absorption has previously been assigned to a superposition of two electronic transitions that involve promotion of an electron from either the highest occupied molecular orbital (HOMO) or the next highest orbital (HOMO-1) of carbazole into the lowest unoccupied orbital (LUMO) of TCNE, as indicated in the figure.

The resonance Raman spectra of the carbazole-TCNE complex show more than 30 lines in the 200–2400 cm^{-1} region assignable as fundamentals (mostly) or combination bands of both carbazole and TCNE vibrations. The absolute cross-sections for these modes were measured at seven wavelengths from 488 to 723 nm (20492 to 13831 cm^{-1}), spanning the charge-transfer absorption.¹²⁰ The absorption spectrum and Raman profiles were simulated with a separable harmonic model for the vibrations that includes two resonant electronic states. When the resonance enhancement involves only a single state, the resonance Raman intensities within a separable harmonic model depend only on the absolute magnitudes of the excited-state geometry changes Δ ; the sign of Δ is irrelevant. However, when two electronic states contribute to the enhancement, the excitation profiles do depend on the *relative* signs of the displacements in the two states because the contributions from the two transitions add at the amplitude level before being squared to give the Raman cross-section. In carbazole:TCNE, some of the Raman profiles are best fit by assuming that the displacements have the same sign in each of the two contributing transitions, whereas others are best fit by assuming opposite signs. Figure 11 shows examples of each.

All of the vibrations assigned to TCNE are best fit with the same sign of Δ in both electronic states. This is expected, as both electronic transitions are believed to involve promotion of an electron into the LUMO of TCNE. However, the profiles for many (not all) of the carbazole vibrations indicate opposite signs for the displacements in the two states. As discussed in ref 120, the signs of the displacements can in most cases be rationalized in terms of the different nodal patterns of the carbazole HOMO and HOMO-1. Those vibrations that involve

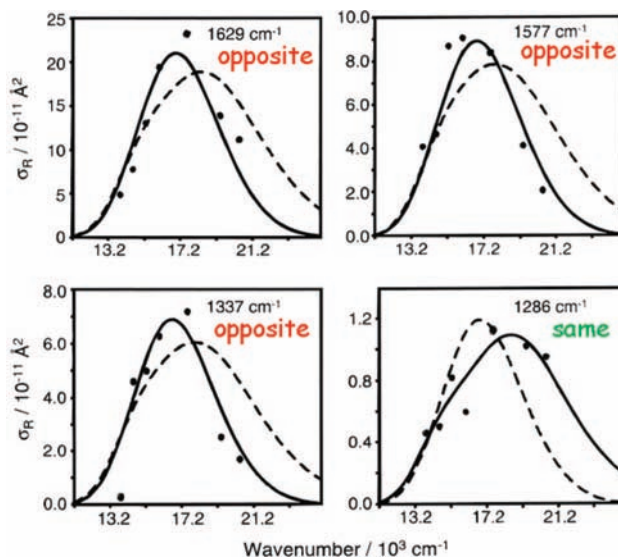


Figure 11. Experimental resonance Raman excitation profiles for four different carbazole vibrations of the 1:1 charge-transfer complex of carbazole with tetracyanoethylene (points), best-fit simulated profiles (solid curve), and profiles calculated using the same parameters but with the sign of the displacement (Δ) in the second electronic state reversed. The 1629, 1577, and 1337 cm^{-1} lines are best fit by assuming opposite signs for Δ in the two states, whereas the 1286 cm^{-1} profile is best fit by assuming displacements of the same sign. Data from ref 120.

primarily stretching of bonds for which the HOMO is bonding and the HOMO-1 is antibonding, or vice versa, are expected and generally observed to have displacements of opposite sign in the two contributing electronic transitions.

Future Development: Experiment. Spontaneous resonance Raman spectroscopy of macroscopic systems is a rather mature field. There exist laser sources that can provide tunable excitation with adequately narrow line widths and adequate power over the range of wavelengths spanned by the low-lying electronic excitations of most interesting molecules (UV to near-IR), and CCD detectors are very good—they have many pixels, are mechanically rugged, and provide low noise and high quantum efficiency in the UV to red. Ion and dye lasers, and low repetition rate pulsed systems such as nanosecond Q-switched Nd:YAG lasers, will increasingly be replaced by solid-state cw and high repetition rate pulsed systems such as diode and Ti:sapphire lasers that are more durable, are more efficient, and do not require external water cooling. There is still a considerable need for less complicated and less expensive laser systems for tunable ultraviolet excitation, as well as for lower noise, higher quantum efficiency detectors for far-red and near-IR excited Raman spectroscopy. There is also a need for improved strategies for laser line rejection that can be tuned over a wide range of laser wavelengths and provide high optical density at the laser wavelength while passing light very close to the laser (small Raman shifts) with high efficiency.

Resonance Raman scattering, which relies on spontaneous emission, is a technique that largely places the experimentalist at Nature's mercy. If the Raman spectrum is weak or extremely complicated, or sits on top of a strong fluorescence background, there is not much that can be done about it. A number of nonlinear spectroscopic techniques, some of which were mentioned above, can provide information similar to that usually sought from resonance Raman spectroscopy, but these techniques have their own complications and limitations and are not the focus of this review.

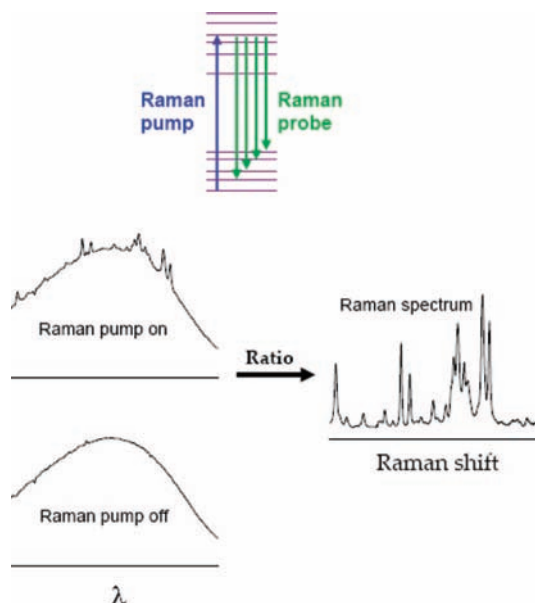


Figure 12. Femtosecond broadband stimulated Raman experiment. A narrow-band Raman pump laser and a broadband Raman probe are simultaneously incident on the sample, producing stimulated Raman scattering over the bandwidth of the probe. Taking the ratio of the probe spectrum with pump present and the probe spectrum in the absence of the pump yields the Raman spectrum. Inspired by Figure 1 of ref 127.

There is, however, one nonlinear technique that is sufficiently similar to spontaneous Raman, and appears sufficiently powerful, that it deserves discussion here: broadband (femtosecond) stimulated Raman scattering, or FSRS.^{124–128} A spectrally narrow (picosecond, $\sim 15\text{ cm}^{-1}$) Raman pump beam and a spectrally very broad (femtosecond, $\sim 1500\text{ cm}^{-1}$) Raman probe beam illuminate the sample simultaneously. The probe beam stimulates Raman scattering excited by the pump, producing sharp Raman lines superimposed on the broadband probe spectrum. Taking the ratio of “pump on” to “pump off” (probe spectrum with Raman lines to probe spectrum alone) produces the Raman spectrum of the sample (Figure 12). The absolute magnitude of the signal (Raman photons per second) is much greater from the stimulated process than from the corresponding spontaneous scattering, and the stimulated signal is produced in the same direction as the probe, allowing the signal to be collected with high efficiency. Consequently, a high-quality Raman spectrum can be collected in a very short period of time compared with spontaneous Raman. As the stimulated Raman lines are usually fairly small features riding on the probe spectrum, it is essential that the probe spectrum be highly stable and reproducible, and FSRS could not have been developed as a useful technique without modern regeneratively amplified Ti:sapphire laser systems whose output meets these requirements.

There is one other major advantage of FSRS over spontaneous Raman for many molecules of interest: FSRS strongly suppresses the fluorescence background. The broadband probe beam stimulates fluorescence as well as Raman, but as long as the pump and probe pulses temporally overlap, the ratio of stimulated Raman to stimulated fluorescence is much greater than the corresponding ratios for the spontaneous processes (because fluorescence persists for nanoseconds after the pump beam has passed, whereas Raman scattering is produced essentially only while the picosecond pump beam is present). When one collects only the stimulated emission, propagating in the same direction as the probe, the fluorescence background can be suppressed by many orders of magnitude. FSRS has been

used to obtain the resonance Raman spectrum of Rhodamine 6G excited at 532 nm, near its absorption maximum. The spontaneous spectrum excited at this wavelength exhibits nothing but fluorescence, but the FSRS spectrum reveals a Raman spectrum with a good signal-to-noise ratio from which absolute Raman cross-sections can be determined by using a methanol solvent band as an internal standard in the usual manner.¹²⁸

Another major direction for future development of this and other optical spectroscopic techniques is in high spatial resolution and imaging applications. Resonance Raman microspectroscopy is becoming a powerful tool for probing chemical compositions and dynamic processes inside complex biological structures^{129–131} and engineered materials.^{132–134} There is also increasing interest in Raman probing with nanometer resolution through near-field and tip-enhanced techniques.¹³⁵ To date, studies that combine resonance enhancement with high spatial resolution typically utilize resonance only as a means of providing selectivity for the chemical species of interest, but one can envision combining spatial resolution with resonance Raman intensity analysis to explore how excited-electronic-state properties are influenced by local environments in spatially heterogeneous systems.

Future Development: Theory. The basic theory of resonance Raman spectroscopy is well developed. Though there are still some areas in which the current state of theory is less than satisfactory—specifically, in describing interactions among multiple resonant or near-resonant electronic surfaces and in handling the effects of solvent dynamics on the scattering process—it appears likely that proper treatment of these effects will require input that is fairly specific to the system of interest and is not easily generalizable.

The most obvious area in which theory will contribute to the interpretation of resonance Raman data in the near future lies in advances in calculations of molecular electronic structure and improved methods for handling the effects of solvent environments on these calculations. The venerable semiempirical methods and their refinements may continue to find applications in calculations on very large extended systems; however, continued advances in computational speed and algorithms will make most systems of interest accessible either through true ab initio electronic structure methods (those that utilize the exact nonrelativistic Born–Oppenheimer Hamiltonian, with a necessarily approximate form for the molecular wave function) or through density functional theory methods (which also use approximations to the electron exchange and electron correlation terms in the full Hamiltonian). Density functional methods have enjoyed tremendous success in recent years in calculating ground-electronic-state properties of even very large molecules, and extensions to excited-electronic-state properties and solvation effects are undergoing rapid development.^{94,95,136–141} The exquisite sensitivity of resonance Raman intensities to the form of the ground-state normal modes and the structure and dynamics of the resonant electronic state(s), and the manner in which these properties are affected by solvation, will make experimental resonance Raman intensities extremely valuable as a benchmark for high-level electronic structure calculations on solvated molecules.

Resonance Hyper-Raman Spectroscopy

Historical Development: Experiment. Electronically non-resonant hyper-Raman scattering (nonlinear inelastic light scattering) was first reported by Terhune, Maker, and Savage in 1965.¹⁴² They utilized a “giant-pulsed” ruby laser (operating

at a repetition rate of two pulses per minute!) and observed hyper-Raman scattering from fused quartz as well as several neat liquids. That work was followed by a number of other hyper-Raman studies, some on neat liquids and most on solids. The first observation of hyper-Raman scattering with a two-photon resonance may have been the work of Horwitz, Kohler, and Spiglanin in 1985 on diphenylbutadiene in a supersonic jet expansion,¹⁴³ although the dispersed spectra were reported only at very low resolution and they did not resemble Raman spectra in the usual sense. The first clear observation of resonance enhanced hyper-Raman scattering was apparently by Ziegler and Roebber on gaseous ammonia in 1987.¹⁴⁴ The Ziegler group went on to publish a number of detailed papers measuring and analyzing the rovibrational resonance hyper-Raman spectra from small molecules in the gas phase at two-photon wavelengths in the far-UV.^{39,145–148} Until much more recently, however, studies of resonance hyper-Raman scattering from molecules in liquids were few.^{149–151} Most resonance hyper-Raman work in solution utilized surface plasmon enhancement on roughened metal electrodes or metallic nanoparticles,^{152–156} which not only greatly enhances the local electromagnetic fields at the adsorbed molecules but also quenches the two-photon excited fluorescence that often interferes with resonance hyper-Raman scattering. A majority of these early experiments were carried out using low repetition rate, nanosecond pulsed Nd:YAG or YAG-pumped dye lasers as excitation sources, although higher repetition rate picosecond lasers were also employed in some studies. In the absence of surface plasmon resonance, signal levels were typically very low and the experiments tended to be plagued by undesirable competing nonlinear processes.

Many of the early solution-phase resonance hyper-Raman experiments were performed on chromophores that have relatively high symmetry and nonpolar or only weakly polar ground states. The early theoretical work of Ziegler et al.¹⁴⁶ had pointed out that the greatest enhancement should be obtained when the resonant excited state is strongly allowed in both one-photon and two-photon absorption. This is most often found in conjugated molecules that are very far from having a center of symmetry. The first experimental study on a molecule of this type may have been the work of Tasumi's group on *all-trans*-retinal.⁴¹ This report was followed shortly by a number of studies from our group on electron donor–acceptor substituted “push-pull” molecules that are known from hyper-Rayleigh scattering and/or electric field induced second harmonic generation (EFISH) to have large first hyperpolarizabilities.^{42–46,48,50,157} Most of the more recent studies utilize high repetition rate picosecond lasers, usually amplified or unamplified Ti:sapphire lasers, although nanosecond pulsed Nd:YAG lasers are still also being used for such experiments. In 2005 our group reported what were apparently the first measurements of absolute resonance hyper-Raman hyperpolarizabilities for molecules in solution, obtained by using the hyper-Rayleigh scattering of neat acetonitrile as an external standard.⁴⁴

Historical Development: Theory. A detailed theoretical analysis of electronically nonresonant hyper-Raman scattering, which included development of the hyper-Raman selection rules and depolarization ratios for most of the important molecular symmetry groups, was presented by Cyvin, Decius, and Rauch in 1965.¹⁵⁸ Long and Stanton, in 1970, discussed the role of electronic resonance in hyper-Raman scattering and presented the general equations governing hyper-Raman scattering with one-photon and/or two-photon resonances.¹⁵⁹ In 1988 Chung and Ziegler presented a conceptually and practically useful development of the general theory analogous to Albrecht's

separation of resonance Raman scattering into A, B, and C terms.¹⁴⁶ The band-integrated differential cross section of the $|i\rangle$ to $|f\rangle$ hyper-Raman transition, in units of $\text{cm}^4 \text{s erg}^{-1}$, is

$$\frac{d\sigma}{d\Omega} = \frac{16\pi^2\alpha^3\nu_s^4}{Nhc^2} |\beta_{ijk}|^2 \quad (7)$$

Here α is the fine structure constant, ν_s is the frequency of the scattered radiation, and i,j,k represent the polarization directions of the incident (two) and scattered photons in the laboratory-fixed frame. The quantity β_{ijk} can be related to the hyperpolarizability components expressed in a molecule-fixed frame, $\beta_{\lambda uv}$, as described, for example, in ref 160. Chung and Ziegler assumed that there is no molecular state resonant or near resonant with one photon of the excitation source, but there is a resonant or near-resonant two-photon state. With this assumption the general theory simplifies considerably, and the hyperpolarizability associated with hyper-Raman scattering can be expressed as a sum of three terms.

$$\beta_{\lambda uv} = A + B + C \quad (8)$$

The A term is given by

$$A = \sum_{s,v} \frac{(M_\lambda)_{ge}^0 (M_\mu)_{es}^0 (M_\nu)_{sg}^0 \langle f|v\rangle \langle v|i\rangle}{(\nu_{gi,s} - \nu_0)(\nu_{gi,ev} - 2\nu_0 - i\Gamma_{gi,ev}/2)} \quad (9)$$

where g is the electronic ground state, e is the two-photon resonant electronic excited state, and s represents any one of the possible one-photon nonresonant electronic states that can serve as intermediate states in the upward two-photon process. ν_0 is the excitation frequency, the v are the vibrational levels of the resonant electronic state, and $(M_\lambda)_{ge}^0$, for example, is the λ component of the purely electronic transition moment between electronic states g and e. The A term is expected to make the most important contribution to the hyper-Raman scattering for noncentrosymmetric molecules, but it is zero for centrosymmetric molecules, as the resonant electronic state e must be allowed in both one-photon absorption [via $(M_\lambda)_{ge}^0$] and through two-photon absorption [via $(M_\mu)_{es}^0 (M_\nu)_{sg}^0$]. The B term contains two purely electronic transition moments and a derivative of one electronic transition moment with respect to a vibrational coordinate and is expected to be the leading term when on resonance with an electronic transition that is either one-photon or two-photon allowed, but not both. The C term involves two transition moment derivatives and can be nonzero even if the resonant electronic state is neither one-photon nor two-photon allowed. Chung and Ziegler estimated that A-term scattering should be about 100 times stronger than the B term which, in turn, should be about 100 times stronger than the C term. These expectations have been borne out by subsequent experiments, which show that resonance hyper-Raman scattering from molecules that are both highly polar and highly polarizable is far stronger than from most more symmetrical conjugated molecules.

Our group has focused on the hyper-Raman scattering from highly noncentrosymmetric “push–pull” conjugated molecules. We have derived explicit expressions for the hyper-Raman hyperpolarizability appropriate for these molecules which include either one, two, or three two-photon resonant or near-resonant electronic states. These expressions, originally derived in the sum-over-states formalism, have been transformed into an equivalent, computationally more efficient time-dependent wavepacket formalism closely related to the time-domain formulation of linear resonance Raman scattering (eq 6).^{44,45} We have also quantitated the importance of paths in the

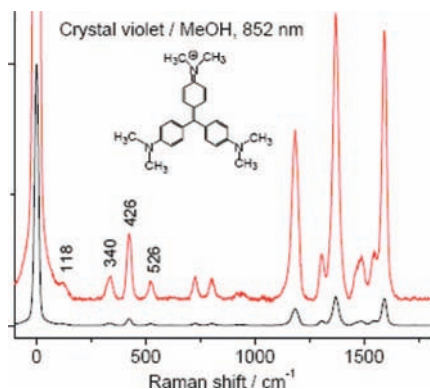


Figure 13. Resonance hyper-Raman spectrum of crystal violet in acetone showing relative intensity of hyper-Rayleigh and hyper-Raman scattering and the ability to detect a low-frequency Raman line at 118 cm^{-1} .

hyperpolarizability that include vibrational levels of the ground state as intermediate states in the upward two-photon process.⁴⁵

Modern Implementation: Experiment. There are still only a few research groups routinely performing two-photon-resonant hyper-Raman spectroscopy in liquid solutions without surface plasmon enhancement. Our group normally employs an unamplified Spectra-Physics Tsunami picosecond Ti:sapphire laser as an excitation source. This relatively simple and reliable laser provides fairly broad tunability (useful power levels from $\sim 720\text{--}960$ nm), a high repetition rate (82 MHz), and good beam quality, and the 1–2 ps pulse duration (~ 15 cm^{-1} spectral width) provides an appropriate balance between peak light intensity and spectral resolution. However, the pulse energies (under 10 nJ/pulse) are rather low for molecules that do not have large hyper-Raman hyperpolarizabilities. The original resonance hyper-Raman work in *all-trans*-retinal by Hamaguchi's group utilized a picosecond Ti:sapphire laser that was regeneratively amplified at 1 kHz.⁴¹ Femtosecond Ti:sapphire lasers are used in many laboratories for time-resolved optical studies but are spectrally too broad to be very useful for hyper-Raman excitation. Ikeda's and Hamaguchi's groups both use spectral filtering to broaden fs Ti:sapphire pulses to ~ 1 ps for hyper-Raman work.^{49,161}

Hyper-Raman scattering has somewhat different requirements for the light collection and detection system than linear resonance Raman. The weakness of the signal places a greater premium on high throughput of the collection optics, spectrograph, and detector. The ratio of signal power to incident laser power is usually many orders of magnitude lower than in linear resonance Raman, but because the signal occurs in a very different wavelength range than the laser, rejection of stray laser light is not usually a problem as it can be in resonance Raman. Simple, inexpensive short-pass filters can block excitation light at 700–1000 nm quite effectively while providing high throughput for the hyper-Raman light at 350–550 nm, and a single spectrograph with a CCD detector completes a highly efficient detection system. The hyper-Rayleigh scattering at twice the laser frequency is rarely strong enough to require filtering, and one of the advantages of the hyper-Raman technique is that observation of low-frequency lines is comparatively easy (Figure 13). Figure 14 diagrams the hyper-Raman apparatus in use in our laboratory.

When accurate hyper-Raman intensities are desired, corrections must be made for the wavelength-dependent collection and detection efficiency and reabsorption of the scattered light in the same manner as for linear resonance Raman. Absolute

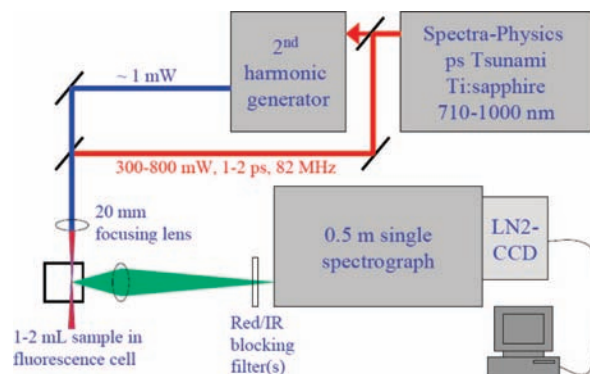


Figure 14. Experimental setup for resonance hyper-Raman and resonance Raman spectroscopy. Either the fundamental (for hyper-Raman) or the attenuated second harmonic (for resonance Raman) of the Ti:sapphire laser can be brought along the same beam path as an excitation source.

hyper-Raman hyperpolarizabilities, however, cannot be obtained by using solvent lines as internal standards for two reasons: there have not, to my knowledge, been any direct measurements of absolute hyper-Raman intensities for electronically nonresonant solvents, and solvent lines are usually not observed in hyper-Raman spectra of two-photon resonant solutes. All common solvents do possess hyper-Raman allowed vibrations, but they are extremely weak at laser powers that avoid saturating the two-photon resonant electronic transitions of the solutes of interest. On the other hand, absolute hyper-Rayleigh hyperpolarizabilities have been measured for a number of pure liquids and solids. We have therefore resorted to using the hyper-Rayleigh scattering from neat acetonitrile as an external standard for resonant hyper-Raman hyperpolarizabilities as described in ref 44 using the absolute hyperpolarizability for acetonitrile reported by Kaatz, Donley, and Shelton.¹⁶² This approach is less than ideal for a number of reasons, including errors arising from fluctuations in the laser power and/or pulse characteristics between temporally separated measurements on sample and reference, the need to know accurately not just the wavelength dependence of the reabsorption correction but its absolute magnitude for the sample spectrum, uncertainties in the primary hyperpolarizability measurement on the solvent, and the lack of wavelength-dependent hyperpolarizability measurements on most solvents. Though there is still a need for better absolute cross-section standards in linear Raman spectroscopy as mentioned above, the need for hyper-Raman scattering is far greater.

Modern Implementation: Theory. To my knowledge, our group is the only one that is currently attempting to analyze and simulate resonance hyper-Raman spectra and excitation profiles. We take an approach similar to that used to determine excited-state parameters from resonance Raman and absorption profiles, described above. In cases where the same resonant electronic state or states contribute to the resonance Raman and resonance hyper-Raman enhancement, the hyper-Raman intensities and excitation profiles depend on the same molecular parameters as do the absorption spectrum and resonance Raman profiles, plus the energies and transition moments involving the intermediate electronic state(s). Thus, it is straightforward to add the resonance hyper-Raman profiles to the other data and seek a set of molecular parameters that give the best global fit to the linear and nonlinear experiments. Similar issues concerning determination of the best fit and choice of model that pertain to simulating linear resonance Raman data carry over to the nonlinear experiments.

Examples. As noted above, the strongest hyper-Raman spectra are observed from noncentrosymmetric molecules whose

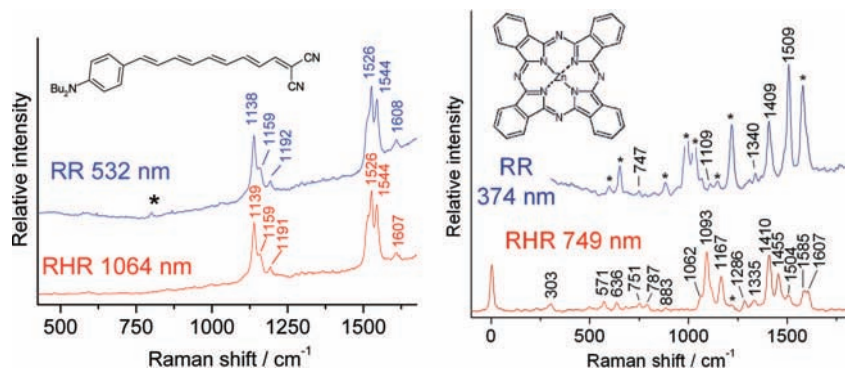


Figure 15. Resonance Raman and resonance hyper-Raman spectra of the molecules shown, at the indicated wavelengths. Asterisks mark solvent lines in the RR spectra.

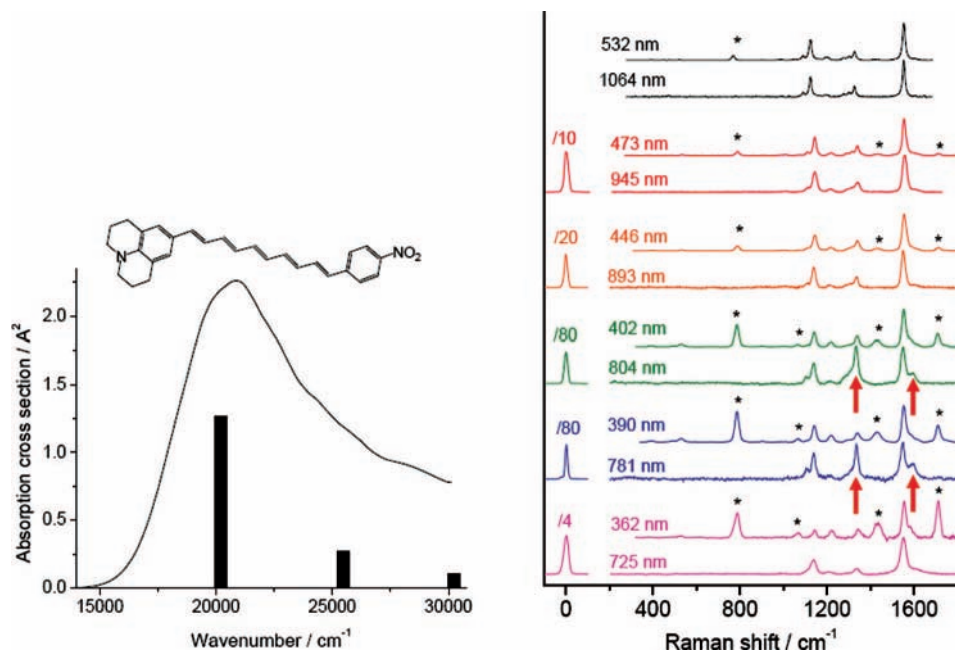


Figure 16. Left: experimental absorption spectrum of the indicated molecule in acetone solution (curve) and predicted positions and one-photon oscillator strengths of the three lowest allowed electronic transitions as obtained from a ZINDO calculation (bars). Right: experimental resonance Raman (upper) and resonance hyper-Raman (lower) spectra at wavelengths spanning this band. Asterisks mark solvent lines in the Raman spectra and red arrows mark two vibrations that have greatly enhanced hyper-Raman intensities at specific excitation regions.

electronic transitions can be simultaneously one-photon and two-photon allowed. When the excitation wavelength is two-photon resonant with a single electronic state, identical intensity patterns are expected in the resonance Raman and resonance hyper-Raman spectra. Figure 15 (left) gives a good example of this for a push–pull substituted conjugated polyene.⁴² The frequencies of the Raman and hyper-Raman peaks are identical to within experimental uncertainty and their relative intensities are essentially identical. It is also possible to observe resonance hyper-Raman scattering from nominally centrosymmetric molecules, where the leading term in the enhancement is the “*B*” term.¹⁴⁶ In this situation the scattering is generally much weaker and one expects complete exclusion between the Raman-active and hyper-Raman active modes, as only modes of “*g*” symmetry can be active in Raman (a two-photon process) whereas only modes of “*u*” symmetry can be active in hyper-Raman (a three-photon process). A good example is zinc phthalocyanine (Figure 15, right), which exhibits only accidental near-degeneracies between Raman and hyper-Raman modes.⁵³ In addition, most of the hyper-Rayleigh scattering observed in solutions of zinc phthalocyanine in pyridine originates from the solvent. The true

hyper-Rayleigh scattering from the chromophore is estimated to be considerably weaker than the strongest hyper-Raman line, in keeping with the expectation that hyper-Rayleigh scattering is strictly forbidden for a truly centrosymmetric molecule.

Resonance hyper-Raman spectroscopy can be particularly valuable for untangling the contributions of overlapping electronic transitions to a broad, unstructured optical absorption band. Figure 16 shows the optical absorption of a conjugated push–pull polyene that is predicted by simple ZINDO electronic structure calculations to have contributions from three major one-photon-allowed electronic transitions. The linear resonance Raman spectra exhibit only modest changes in relative intensities as the excitation is tuned across the broad absorption band. The resonance hyper-Raman spectra are nearly identical to the resonance Raman spectra at most excitation wavelengths, but in the 390–400 nm region two bands appear with greatly enhanced intensities in the hyper-Raman spectra. These are assigned as the symmetric NO₂ stretch and a phenyl group vibration, indicating that the electronic transition near 400 nm has a greater relative two-photon absorption strength compared with the other contrib-

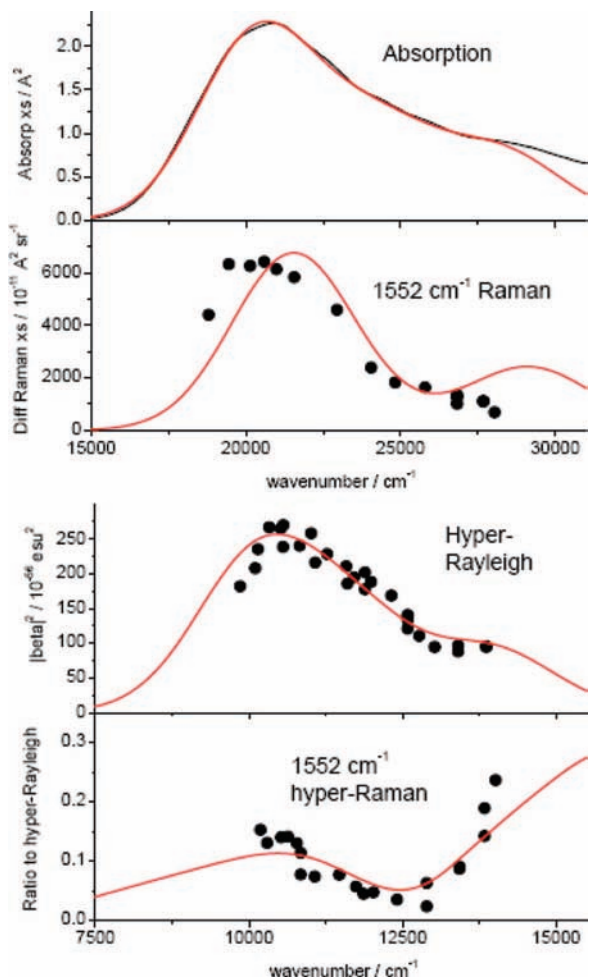


Figure 17. Experimental (solid curve and black points) and simulated (red curves) data for the molecule in Figure 16. Shown are the linear absorption spectrum, resonance Raman excitation profile for the strongest C=C stretching mode, hyper-Rayleigh excitation profile, and ratio of hyper-Raman to hyper-Rayleigh for the same C=C stretch. Parameters of the fits are given in ref 45.

uting transitions and is localized on the nitrophenyl moiety. Quantitative simulation of the absorption, resonance Raman, hyper-Raman, and hyper-Rayleigh profiles (Figure 17) provides excited-state geometry changes in each of the three contributing transitions, which could not have been obtained from the absorption and resonance Raman spectra alone.⁴⁵

Future Development: Experiment. Resonance hyper-Raman spectroscopy seems unlikely to ever become a very common technique owing to the general weakness of the effect. Its value is likely to be found in certain “niche” applications. As outlined above, hyper-Raman intensities provide useful information on the physical origin of nonlinear optical responses and it is likely that this will remain a fruitful avenue of investigation for some time in the future.

Compared with most spectroscopic techniques, hyper-Raman scattering exhibits a very large range of signal strengths between a strong, electronically resonant scatterer and a weak or electronically nonresonant scatterer. Although this renders the technique not very general, it also makes it highly selective: signal from a strong resonance hyper-Raman scatterer can be seen with little interference from other molecules present at far higher concentrations in the sample. Hyper-Raman “labels” could, in principle, replace fluorescent tags in certain biological or other analytical applications. Hyper-Raman scattering should have some of the same advantages for imaging applications as

multiphoton excited fluorescence: improved spatial resolution because of the dependence of the signal on the square of the incident light intensity, the ability to penetrate fairly deeply into biological or turbid materials with red- or near-IR excitation (although the signal at shorter wavelengths still has to get out), minimal sample photodamage from the low-energy excitation photons, and large separation between the signal and laser wavelengths allowing a rather simple and compact detection system. If an analyte of interest contains or can easily be labeled with a strong hyper-Raman chromophore, hyper-Raman could be an excellent way to probe it.

Several experimental extensions of hyper-Raman scattering may prove interesting. It is well-known that sum frequency generation can be a much more flexible and informative tool than its degenerate analog, second harmonic generation. Similarly, spontaneous hyper-Raman scattering performed with two different excitation frequencies ($\omega_S = \omega_1 + \omega_2 - \omega_{\text{vib}}$) would allow probing of intermediate resonances in the two-photon excitation process^{50,163–166} as well as independent selection of the polarizations of both incident fields and the scattered field. I do not know of any such nondegenerate spontaneous hyper-Raman experiments but they should pose no fundamental difficulties beyond the additional complexity associated with spatially and temporally overlapping two independently tunable excitation pulses. A second obvious extension is the three-photon analog where $\omega_S = 3\omega_L - \omega_{\text{vib}}$. It is not clear, however, that this process would be particularly informative as anything but a proof of principle experiment because of the usually identical selection rules between it and linear Raman.

Future Development: Theory. The fundamental theory of resonance hyper-Raman scattering is considerably less well developed than for resonance Raman. By this I mean that it is not yet clear what approximations can safely be made to the most general expression for the hyper-Raman hyperpolarizability. For example, in our group’s early work we assumed that vibrational levels of the ground electronic state would not contribute importantly as nonresonant intermediate states in the two-photon excitation process.⁴⁴ However, motivated by work indicating that these terms may make important contributions to the nonresonant hyper-Rayleigh hyperpolarizability (“vibrational hyperpolarizability”), we subsequently incorporated them into the resonance hyper-Raman calculations and found that these paths could be important for certain vibrations that are strongly infrared active.⁴⁵

Largely because of the strong interest in developing materials with large nonlinear optical coefficients for technological applications, there have been many experimental studies of hyper-Rayleigh hyperpolarizabilities (mostly in the electronically nonresonant regime) as well as calculations of hyperpolarizabilities and their variation with molecular structure, solvent, and in some cases wavelength.^{106,167–173} There have been a few reported calculations of hyper-Raman spectra, but only, to my knowledge, in the electronically nonresonant limit.^{174,175} Quantum chemical calculations of hyper-Raman spectra and hyperpolarizabilities with two-photon electronic resonance constitute a very challenging problem for electronic structure theory in the future.

Acknowledgment. This work was made possible by grants from a number of agencies, particularly NSF, and by the work of many undergraduates, graduate students, postdoctoral fellows, and senior collaborators. Julien Guthmuller and Benoît Champagne provided the original calculated data used to plot Figure 8.

References and Notes

- (1) Mortensen, O. S.; Hassing, S. *Adv. Infrared Raman Spectrosc.* **1980**, *6*, 1.
- (2) Placzek, G. In *Handbuch der Radiologie*; Marx, E., Ed.; Akademische Verlagsgesellschaft: Leipzig, 1934; Vol. 6, p 205.
- (3) Long, D. A. *Raman Spectroscopy*; McGraw-Hill: New York, 1977.
- (4) Myers, A. B.; Mathies, R. A. In *Biological Applications of Raman Spectroscopy*; Spiro, T. G., Ed.; Wiley: New York, 1987; Vol. 2, p 1.
- (5) Hupp, J. T.; Williams, R. D. *Acc. Chem. Res.* **2001**, *34*, 808.
- (6) Myers, A. B. In *Laser Techniques in Chemistry*; Myers, A. B., Rizzo, T. R., Eds.; Wiley: New York, 1995; p 325.
- (7) McHale, J. L. *Acc. Chem. Res.* **2001**, *34*, 265.
- (8) Terner, J.; El-Sayed, M. A. *Acc. Chem. Res.* **1985**, *18*, 331.
- (9) Hogiu, S.; Werncke, W.; Pfeiffer, M.; Elsaesser, T. *Chem. Phys. Lett.* **1999**, *312*, 407.
- (10) Pan, D.; Mathies, R. A. *Biochem.* **2001**, *40*, 7929.
- (11) Godbout, J. T.; Pietrzykowski, M. D.; Gould, I. R.; Goodman, J. L.; Kelley, A. M. *J. Phys. Chem. A* **1999**, *103*, 3876.
- (12) Hayes, S. C.; Philpott, M. P.; Mayer, S. G.; Reid, P. J. *J. Phys. Chem. A* **1999**, *103*, 5534.
- (13) Reid, P. J.; Doig, S. J.; Wickham, S. D.; Mathies, R. A. *J. Am. Chem. Soc.* **1993**, *115*, 4754.
- (14) Beck, S. M.; Brus, L. E. *J. Am. Chem. Soc.* **1982**, *104*, 1805.
- (15) Gustafson, T. L.; Iwata, K.; Weaver, W. L.; Huston, L. A.; Benson, R. L. In *Laser Applications in Life Sciences. Proc. SPIE 1403*; Akmanov, S. A., Povoshina, M. Y., Eds.; SPIE: Bellingham, WA, 1991.
- (16) Gustafson, T. L.; Roberts, D. M.; Chernoff, D. A. *J. Chem. Phys.* **1983**, *79*, 1559.
- (17) Petrich, J. W.; Martin, J. L.; Houde, D.; Poyart, C.; Orszag, A. *Biochemistry* **1987**, *26*, 7914.
- (18) Cheng, J.-X.; Xie, X. S. *J. Phys. Chem. B* **2004**, *108*, 827.
- (19) Levenson, M. D. *Introduction to nonlinear laser spectroscopy*; Academic Press: New York, 1982.
- (20) Shen, Y. R. *The principles of nonlinear optics*; John Wiley & Sons: New York, 1984.
- (21) *Advances in Nonlinear Spectroscopy*; Clark, R. J. H., Hester, R. E., Eds.; Wiley: New York, 1988.
- (22) Pollard, W. T.; Dexheimer, S. L.; Wang, Q.; Peteanu, L. A.; Shank, C. V.; Mathies, R. A. *J. Phys. Chem.* **1992**, *96*, 6147.
- (23) Jonas, D. M.; Bradforth, S. E.; Passino, S. A.; Fleming, G. R. *J. Phys. Chem.* **1995**, *99*, 2594.
- (24) Gruia, F.; Kubo, M.; Ye, X.; Lonascu, D.; Lu, C.; Poole, R. K.; Yeh, S.-R.; Champion, P. M. *J. Am. Chem. Soc.* **2008**, *130*, 5231.
- (25) Shelly, K. R.; Golovich, E. C.; Dillman, K. L.; Beck, W. F. *J. Phys. Chem. B* **2008**, *112*, 1299.
- (26) Qian, X.-M.; Nie, S. M. *Chem. Soc. Rev.* **2008**, *37*, 912.
- (27) Kneipp, J.; Kneipp, H.; Kneipp, K. *Chem. Soc. Rev.* **2008**, *37*, 1052.
- (28) Jensen, L.; Aikens, C. M.; Schatz, G. C. *Chem. Soc. Rev.* **2008**, *37*, 1061.
- (29) Tian, Z.-Q.; Ren, B.; Wu, D.-Y. *J. Phys. Chem. B* **2002**, *106*, 9463.
- (30) Moskovits, M. *J. Raman Spectrosc.* **2005**, *36*, 485.
- (31) Campion, A.; Kambhampati, P. *Chem. Soc. Rev.* **1998**, *27*, 241.
- (32) Le Ru, E. C.; Blackie, E.; Meyer, M.; Etchegoin, P. G. *J. Phys. Chem. C* **2007**, *111*, 13794.
- (33) Kelley, A. M. *J. Chem. Phys.* **2008**, *128*, 224702.
- (34) Lombardi, J. R.; Birke, R. L. *J. Chem. Phys.* **2007**, *126*, 244709.
- (35) Lombardi, J. R.; Birke, R. L. *J. Phys. Chem. C* **2008**, *112*, 5605.
- (36) Gibson, J. W.; Johnson, B. R. *J. Chem. Phys.* **2006**, *124*, 064701.
- (37) Lee, M. T.; Wu, D. Y.; Tian, Z. Q.; Lin, S. H. *J. Chem. Phys.* **2005**, *122*, 094719.
- (38) Denisov, V. N.; Martin, B. N.; Podobedov, V. B. *Phys. Rep.* **1987**, *151*, 1.
- (39) Ziegler, L. D. *J. Raman Spectrosc.* **1990**, *21*, 769.
- (40) Itoh, T.; Ozaki, Y.; Yoshikawa, H.; Ihama, T.; Masuhara, H. *Appl. Phys. Lett.* **2006**, *88*, 084102.
- (41) Mizuno, M.; Hamaguchi, H.; Tahara, T. *J. Phys. Chem. A* **2002**, *106*, 3599.
- (42) Kelley, A. M.; Leng, W.; Blanchard-Desce, M. *J. Am. Chem. Soc.* **2003**, *125*, 10520.
- (43) Shoute, L. C. T.; Blanchard-Desce, M.; Kelley, A. M. *J. Chem. Phys.* **2004**, *121*, 7045.
- (44) Shoute, L. C. T.; Bartholomew, G. P.; Bazan, G. C.; Kelley, A. M. *J. Chem. Phys.* **2005**, *122*, 184508.
- (45) Shoute, L. C. T.; Blanchard-Desce, M.; Kelley, A. M. *J. Phys. Chem. A* **2005**, *109*, 10503.
- (46) Shoute, L. C. T.; Woo, H. Y.; Vak, D.; Bazan, G. C.; Kelley, A. M. *J. Chem. Phys.* **2006**, *125*, 054506.
- (47) Shimada, R.; Kano, H.; Hamaguchi, H. *J. Raman Spectrosc.* **2006**, *37*, 469.
- (48) Shoute, L. C. T.; Helburn, R.; Kelley, A. M. *J. Phys. Chem. A* **2007**, *111*, 1251.
- (49) Ikeda, K.; Saito, Y.; Hayazawa, N.; Kawata, S.; Uosaki, K. *Chem. Phys. Lett.* **2007**, *438*, 109.
- (50) Leng, W.; Kelley, A. M. *J. Chem. Phys.* **2007**, *127*, 164509.
- (51) Kelley, A. M.; Shoute, L. C. T. In *Ultrafast Phenomena XV*; Corkum, P., Jonas, D., Miller, R. J. D., Weiner, A. M., Eds.; Springer-Verlag: Berlin, Heidelberg, 2007; p 519.
- (52) Ikeda, K.; Uosaki, K. *J. Phys. Chem. A* **2008**, *112*, 790.
- (53) Leng, W.; Kelley, A. M. *J. Phys. Chem. A* **2008**, *112*, 5925.
- (54) Raman, C. V. *Nature* **1928**, *121*, 619.
- (55) Raman, C. V.; Krishnan, K. S. *Nature* **1928**, *121*, 501.
- (56) Murphy, W. F.; Holzer, W.; Bernstein, H. *J. Appl. Spectrosc.* **1969**, *23*, 211.
- (57) Kramers, H. A.; Heisenberg, W. *Z. Phys.* **1925**, *31*, 681.
- (58) Dirac, P. A. M. *Proc. Roy. Soc. (London)* **1927**, *114*, 710.
- (59) Albrecht, A. C. *J. Chem. Phys.* **1961**, *34*, 1476.
- (60) Albrecht, A. C.; Hutley, M. C. *J. Chem. Phys.* **1971**, *55*, 4438.
- (61) Tang, J.; Albrecht, A. C. In *Raman Spectroscopy*; Szymanski, H. A., Ed.; Plenum: New York, 1970; Vol. 2; p 33.
- (62) Myers, A. B. *Annu. Rev. Phys. Chem.* **1998**, *49*, 267.
- (63) Hochstrasser, R. M.; Nyi, C. A. *J. Chem. Phys.* **1979**, *70*, 1112.
- (64) Fujimura, Y.; Kono, H.; Nakajima, T.; Lin, S. H. *J. Chem. Phys.* **1981**, *75*, 99.
- (65) Lee, D.; Albrecht, A. C. *Adv. Infrared Raman Spectrosc.* **1985**, *12*, 179.
- (66) Mukamel, S. *J. Chem. Phys.* **1985**, *82*, 5398.
- (67) Sue, J.; Yan, Y. J.; Mukamel, S. *J. Chem. Phys.* **1986**, *85*, 462.
- (68) Yan, Y. J.; Mukamel, S. *J. Chem. Phys.* **1987**, *86*, 6085.
- (69) Myers, A. B.; Trulson, M. O.; Mathies, R. A. *J. Chem. Phys.* **1985**, *83*, 5000.
- (70) Myers, A. B.; Trulson, M. O.; Pardo, J. A.; Heeremans, C.; Lugtenburg, J.; Mathies, R. A. *J. Chem. Phys.* **1986**, *84*, 633.
- (71) Lee, S.-Y.; Heller, E. J. *J. Chem. Phys.* **1979**, *71*, 4777.
- (72) Heller, E. J.; Sundberg, R. L.; Tannor, D. J. *J. Phys. Chem.* **1982**, *86*, 1822.
- (73) Myers, A. B.; Mathies, R. A.; Tannor, D. J.; Heller, E. J. *J. Chem. Phys.* **1982**, *77*, 3857.
- (74) Tannor, D. J.; Heller, E. J. *J. Chem. Phys.* **1982**, *77*, 202.
- (75) Myers, A. B.; Harris, R. A.; Mathies, R. A. *J. Chem. Phys.* **1983**, *79*, 603.
- (76) Kim, M.; Owen, H.; Carey, P. R. *Appl. Spectrosc.* **1993**, *47*, 1780.
- (77) McCreery, R. L. *Raman Spectroscopy for Chemical Analysis*; Wiley-Interscience: New York, 2000.
- (78) Chase, D. B. *J. Am. Chem. Soc.* **1986**, *108*, 7485.
- (79) Nakashima, S.-I.; Okumura, H.; Yamamoto, T.; Shimidzu, R. *Appl. Spectrosc.* **2004**, *58*, 224.
- (80) Schulz, B.; Backstrom, J.; Budelmann, D.; Maeser, R.; Rubhausen, M.; Klein, M. V.; Schoeffel, E.; Mihill, A.; Yoon, S. *Rev. Sci. Instrum.* **2005**, *76*, 073107.
- (81) Russell, M. P.; Vohnik, S.; Thomas, G. J. *Biophys. J.* **1995**, *68*, 1607.
- (82) Efremov, E. V.; Buijs, J. B.; Gooijer, C.; Ariese, F. *Appl. Spectrosc.* **2007**, *61*, 571.
- (83) Mandal, D.; Mizuno, M.; Tahara, T. *J. Mol. Struct.* **2005**, *735*, 189.
- (84) Everall, N.; Jackson, R. W.; Howard, J.; Hutchinson, K. *J. Raman Spectrosc.* **1986**, *17*, 415.
- (85) Matousek, P.; Towrie, M.; Stanley, A.; Parker, A. W. *Appl. Spectrosc.* **1999**, *53*, 1485.
- (86) Kato, Y.; Takuma, H. *J. Opt. Soc. Am.* **1971**, *61*, 347.
- (87) Schomacker, K. T.; Delaney, J. K.; Champion, P. M. *J. Chem. Phys.* **1986**, *85*, 4240.
- (88) Trulson, M. O.; Mathies, R. A. *J. Chem. Phys.* **1986**, *84*, 2068.
- (89) Li, B.; Myers, A. B. *J. Phys. Chem.* **1990**, *94*, 4051.
- (90) Shreve, A. P.; Mathies, R. A. *J. Phys. Chem.* **1995**, *99*, 7265.
- (91) Lilichenko, M.; Kelley, A. M. *J. Chem. Phys.* **2001**, *114*, 7094.
- (92) Hennessy, M. H.; Kelley, A. M. *J. Phys. Chem. Chem. Phys.* **2004**, *6*, 1085.
- (93) Shorr, E.; Kelley, A. M. *J. Phys. Chem. Chem. Phys.* **2007**, *9*, 4785.
- (94) Guthmuller, J.; Champagne, B. *J. Chem. Phys.* **2007**, *127*, 164507.
- (95) Jensen, L.; Schatz, G. C. *J. Phys. Chem. A* **2006**, *110*, 5973.
- (96) Neugebauer, J.; Hess, B. A. *J. Chem. Phys.* **2004**, *120*, 11564.
- (97) Neugebauer, J.; Baerends, E. J.; Efremov, E. V.; Ariese, F.; Gooijer, C. *J. Phys. Chem. A* **2005**, *109*, 2100.
- (98) Yamashita, T.; Kato, S. *Chem. Phys. Lett.* **2005**, *405*, 142.
- (99) Ben-Nun, M.; Martinez, T. J. *J. Phys. Chem. A* **1999**, *103*, 10517.
- (100) Moran, A. M.; Delbecq, C.; Kelley, A. M. *J. Phys. Chem. A* **2001**, *105*, 10208.
- (101) Painelli, A.; Del Freo, L.; Terenziani, F. *Chem. Phys. Lett.* **2001**, *346*, 470.
- (102) Painelli, A.; Terenziani, F. *Synth. Met.* **2001**, *116*, 135.

- (103) Moran, A. M.; Egolf, D. S.; Blanchard-Desce, M.; Kelley, A. M. *J. Chem. Phys.* **2002**, *116*, 2542.
- (104) Moran, A. M.; Blanchard-Desce, M.; Kelley, A. M. *Chem. Phys. Lett.* **2002**, *358*, 320.
- (105) Drobizhev, M.; Makarov, N. S.; Rebane, A.; de la Torre, G.; Torres, T. *J. Phys. Chem. C* **2008**, *112*, 848.
- (106) Chafin, A. P.; Lindsay, G. A. *J. Phys. Chem. C* **2008**, *112*, 7829.
- (107) Moran, A. M.; Kelley, A. M. *J. Chem. Phys.* **2001**, *115*, 912.
- (108) Moran, A. M.; Bartholomew, G. P.; Bazan, G. C.; Kelley, A. M. *J. Phys. Chem. A* **2002**, *106*, 4928.
- (109) Leng, W.; Wang, C. H.; Asato, A. E.; Kelley, A. M. *J. Phys. Chem. A* **2002**, *106*, 9479.
- (110) Rosenthal, S. J.; Xie, X.; Du, M.; Fleming, G. R. *J. Chem. Phys.* **1991**, *95*, 4715.
- (111) Myers, A. B. *Chem. Phys.* **1994**, *180*, 215.
- (112) Kelley, A. M. *J. Phys. Chem. A* **1999**, *103*, 6891.
- (113) Cao, X.; McHale, J. L. *J. Chem. Phys.* **1998**, *109*, 1901.
- (114) Wootton, J. L.; Zink, J. I. *J. Am. Chem. Soc.* **1997**, *119*, 1895.
- (115) Fraga, E.; Webb, M. A.; Loppnow, G. R. *J. Phys. Chem.* **1996**, *100*, 3278.
- (116) Blackburn, R. L.; Johnson, C. S.; Hupp, J. T. *J. Am. Chem. Soc.* **1991**, *113*, 1060.
- (117) Wright, P. G.; Stein, P.; Burke, J. M.; Spiro, T. G. *J. Am. Chem. Soc.* **1979**, *101*, 3531.
- (118) Britt, B. M.; McHale, J. L.; Friedrich, D. M. *J. Phys. Chem.* **1995**, *99*, 6347.
- (119) Kulinowski, K.; Gould, I. R.; Myers, A. B. *J. Phys. Chem.* **1995**, *99*, 9017.
- (120) Egolf, D. S.; Waterland, M. R.; Kelley, A. M. *J. Phys. Chem. B* **2000**, *104*, 10727.
- (121) Markel, F.; Ferris, N. S.; Gould, I. R.; Myers, A. B. *J. Am. Chem. Soc.* **1992**, *114*, 6208.
- (122) Lilichenko, M.; Tittelbach-Helmrich, D.; Verhoeven, J. W.; Gould, I. R.; Myers, A. B. *J. Chem. Phys.* **1998**, *109*, 10958.
- (123) Lilichenko, M.; Kelley, A. M. *J. Chem. Phys.* **1999**, *111*, 2345.
- (124) Kukura, P.; McCamant, D. W.; Mathies, R. A. *J. Phys. Chem. A* **2004**, *108*, 5921.
- (125) Lee, S.-Y.; Zhang, D.; McCamant, D. W.; Kukura, P.; Mathies, R. A. *J. Chem. Phys.* **2004**, *121*, 3632.
- (126) Kukura, P.; Yoon, S.; Mathies, R. A. *Anal. Chem.* **2006**, *78*, 5952.
- (127) McCamant, D. W.; Kukura, P.; Mathies, R. A. *Appl. Spectrosc.* **2003**, *57*, 1317.
- (128) Shim, S.; Stuart, C. M.; Mathies, R. A. *ChemPhysChem* **2008**, *9*, 697.
- (129) Frosch, T.; Schmitt, M.; Noll, T.; Bringmann, G.; Schenzel, K.; Popp, J. *Anal. Chem.* **2007**, *79*, 986.
- (130) van Manen, H. J.; Kraan, Y. M.; Roos, D.; Otto, C. *J. Phys. Chem. B* **2004**, *108*, 18762.
- (131) Sijtsema, N. M.; Otto, C.; Segers-Nolten, G. M. J.; Verhoeven, A. J.; Greve, J. *Biophys. J.* **1998**, *74*, 3250.
- (132) Cronin, S. B.; Swan, A. K.; Unlu, M. S.; Goldberg, B. B.; Dresselhaus, M. S.; Tinkham, M. *Phys. Rev. Lett.* **2004**, *93*, 167401.
- (133) Stangar, U. L.; Orel, B.; Vuk, A. S.; Sagon, G.; Colombari, P.; Stathatos, E.; Lianos, P. *J. Electrochem. Soc.* **2002**, *149*, E413.
- (134) Klimov, E.; Li, W.; Yang, X.; Hoffmann, G. G.; Loos, J. *Macromolecules* **2006**, *39*, 4493.
- (135) Zhang, W.; Yeo, B. S.; Schmid, T.; Zenobi, R. *J. Phys. Chem. C* **2007**, *111*, 1733.
- (136) Nguyen, K. A.; Day, P. N.; Pachter, R. *J. Chem. Phys.* **2007**, *126*, 094303.
- (137) Clark, A. E.; Qin, C.; Li, A. D. Q. *J. Am. Chem. Soc.* **2007**, *129*, 7586.
- (138) Badaeva, E.; Tretiak, S. *Chem. Phys. Lett.* **2008**, *450*, 322.
- (139) Jha, P. C.; Minaev, B.; Ågren, H. *J. Chem. Phys.* **2008**, *128*, 074302.
- (140) Guthmuller, J.; Champagne, B. *J. Phys. Chem. A* **2008**, *112*, 3215.
- (141) Burke, K.; Werschnik, J.; Gross, E. K. U. *J. Chem. Phys.* **2005**, *123*, 062206.
- (142) Terhune, R. W.; Maker, P. D.; Savage, C. M. *Phys. Rev. Lett.* **1965**, *14*, 681.
- (143) Horwitz, J. S.; Kohler, B. E.; Spiglanin, T. A. *J. Phys. Chem.* **1985**, *89*, 1574.
- (144) Ziegler, L. D.; Roebber, J. L. *Chem. Phys. Lett.* **1987**, *136*, 377.
- (145) Chung, Y. C.; Ziegler, L. D. *J. Chem. Phys.* **1988**, *89*, 4692.
- (146) Chung, Y. C.; Ziegler, L. D. *J. Chem. Phys.* **1988**, *88*, 7287.
- (147) Ziegler, L. D.; Chung, Y. C.; Zhang, Y. P. *J. Chem. Phys.* **1987**, *87*, 4498.
- (148) Campbell, D. J.; Ziegler, L. D. *J. Chem. Phys.* **1993**, *98*, 150.
- (149) Bonang, C. C.; Cameron, S. M. *J. Chem. Phys.* **1992**, *97*, 5377.
- (150) Bonang, C. C.; Cameron, S. M. *Chem. Phys. Lett.* **1992**, *192*, 303.
- (151) Bonang, C. C.; Cameron, S. M. *Chem. Phys. Lett.* **1991**, *187*, 619.
- (152) Nie, S.; Lipscomb, L. A.; Feng, S.; Yu, N.-T. *Chem. Phys. Lett.* **1990**, *167*, 35.
- (153) Baranov, A. V.; Bobovich, Y. S.; Petrov, V. I. *J. Raman Spectrosc.* **1993**, *24*, 695.
- (154) Kneipp, K.; Kneipp, H.; Seifert, F. *Chem. Phys. Lett.* **1995**, *233*, 519.
- (155) Schneider, S.; Brehm, G.; Freunsch, P. *Phys. Stat. Sol. B* **1995**, *189*, 37.
- (156) Li, W.-H.; Li, X.-Y.; Yu, N.-T. *Chem. Phys. Lett.* **1999**, *312*, 28.
- (157) Kelley, A. M.; Shoute, L. C. T.; Blanchard-Desce, M.; Bartholomew, G. P.; Bazan, G. C. *Mol. Phys.* **2006**, *104*, 1239.
- (158) Cyvin, S. J.; Rauch, J. E.; Decius, J. C. *J. Chem. Phys.* **1965**, *43*, 4083.
- (159) Long, D. A.; Stanton, L. *Proc. R. Soc. London, A* **1970**, *318*, 441.
- (160) Kauranen, M.; Persoons, A. *J. Chem. Phys.* **1996**, *104*, 3445.
- (161) Shimada, R.; Kano, H.; Hamaguchi, H. *Opt. Lett.* **2006**, *31*, 320.
- (162) Kaatz, P.; Donley, E. A.; Shelton, D. P. *J. Chem. Phys.* **1998**, *108*, 849.
- (163) Drobizhev, M.; Meng, F.; Rebane, A.; Stepanenko, Y.; Nickel, E.; Spangler, C. W. *J. Phys. Chem. B* **2006**, *110*, 9802.
- (164) Drobizhev, M.; Makarov, N. S.; Hughes, T.; Rebane, A. *J. Phys. Chem. B* **2007**, *111*, 14051.
- (165) Johnsen, M.; Paterson, M. J.; Arnbjerg, J.; Christiansen, O.; Nielsen, C. B.; Jorgensen, M.; Ogilby, P. R. *Phys. Chem. Chem. Phys.* **2008**, *10*, 1177.
- (166) Hales, J. M.; Hagan, D. J.; Van Stryland, E. W.; Schaefer, K. J.; Morales, A. R.; Belfield, K. D.; Pacher, P.; Kwon, O.; Zojer, E.; Bredas, J. L. *J. Chem. Phys.* **2004**, *121*, 3152.
- (167) Bokhan, D.; Bartlett, R. J. *J. Chem. Phys.* **2007**, *127*, 174102.
- (168) Kang, H.; Facchetti, A.; Jiang, H.; Cariati, E.; Righetto, S.; Ugo, R.; Zuccaccia, C.; Macchioni, A.; Stern, C. L.; Liu, Z.; Ho, S.-T.; Brown, E. C.; et al. *J. Am. Chem. Soc.* **2007**, *129*, 3267.
- (169) Isborn, C. M.; Leclercq, A.; Vila, F. D.; Dalton, L. R.; Bredas, J. L.; Eichinger, B. E.; Robinson, B. H. *J. Phys. Chem. A* **2007**, *111*, 1319.
- (170) Guthmuller, J.; Simon, D. *J. Chem. Phys.* **2006**, *124*, 174502.
- (171) Jensen, L.; van Duijnen, P. T.; Snijders, J. G. *J. Chem. Phys.* **2003**, *119*, 12998.
- (172) Jensen, L.; van Duijnen, P. T. *J. Chem. Phys.* **2005**, *123*, 074307.
- (173) Reis, H.; Grzybowski, A.; Papadopoulos, M. G. *J. Phys. Chem. A* **2005**, *109*, 10106.
- (174) Quinet, O.; Champagne, B. *J. Chem. Phys.* **2002**, *117*, 2481.
- (175) Quinet, O.; Champagne, B.; Rodriguez, V. *J. Chem. Phys.* **2004**, *121*, 4705.